TURBOMACHINERY & PUMP SYMPOSIA | HOUSTON, TX
SEPTEMBER 13-15, 2022
SHORT COURSES: SEPTEMBER 12, 2022

AN OVERVIEW OF THE DESIGN AND PERFORMANCE TESTING OF A 275 BAR INTEGRALLY GEARED SUPERCRITICAL CO_2 COMPRESSOR FOR POWER GENERATION

Jason C. Wilkes, Ph.D.
Manager
Southwest Research Institute
San Antonio, TX, USA

Robert Pelton
Engineering Manager
Hanwha Power Systems
Americas
Houston, TX, USA

Karl Wygant, Ph.D.
C.O.O.
Hanwha Power Systems
Americas Houston, TX, USA

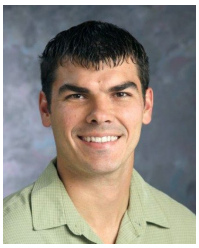

Dr. Jason Wilkes is a Manager of the Rotating Machinery Dynamics Section at Southwest Research Institute (SwRI) in San Antonio, TX. His experience at SwRI includes design and construction of various test rigs, predicting lateral and torsional rotordynamic analyses, bearings and seals, and auxiliary bearing dynamics following failure of AMB supported turbomachinery. Dr. Wilkes holds a B.S., M.S., and Ph.D. in Mechanical Engineering from Texas A&M University where he worked at the Turbomachinery Laboratory for six years.

Robert Pelton is the Engineering Manager of the Design and Development Group at Hanwha Power Systems (Hanwha), in Houston, TX. He oversees a team responsible for the analytic design of new products, including the aerodynamic, structural, and rotordynamic performance of multi-stage integrally geared compressors. He holds a B.S. and M.S. in Mechanical Engineering from Brigham Young University. Prior to coming to Hanwha, Mr. Pelton worked at Concepts NREC on the aerodynamic design of a wide range of turbomachinery including radial compressors, pumps and turbines.

Dr. Karl Wygant is the Chief Operating Officer for Hanwha Power System America's Design and Development Center located in Houston, TX. Dr. Wygant holds an M.S. and Ph.D. in Mechanical Engineering from the University of Virginia and an M.B.A. from Norwich University. His engineering experience over the last 25 years is related to a wide variety of turbomachinery including: rocket-turbopumps, automotive turbochargers, industrial compressors, steam turbines, gas turbines, and novel turbo-machimery applications. His management background includes: project management, multi-group management, business management, and leading new product development from inception to market delivery.

ABSTRACT

An integrally geared compressor-expander (compander) for supercritical CO_2 (sCO_2) was developed to convert thermal energy to electricity. With operating pressures of 275 bar, this turbomachine represents the state of the art in integrally geared machine architecture, hitting compressor inlet densities of 600 kg/m^3 and discharge pressures of 275 bar. The product development was funded by the Department of Energy's Energy Efficiency and Renewable Energy Office under EE0007114 to advance the state of the art in concentrated solar power applications; however, the technology itself is agnostic to heat source, and is predicted to achieve a thermal-to-electric conversion efficiency of 50% for any indirect heat source capable of providing turbine inlet temperatures of 700°C or greater.

While the program encompassed the design and testing for the compressor and turbine elements, this paper will focus on the compressor design and operation. The paper will begin with an introduction to the cycle design and analysis of an indirectly heated integrally geared sCO_2 compander, a discussion of the mechanical and aerodynamic design of the compressor that is a two stage radial compressor operating subcritically at 27,512 rpm, and will then proceed to describe the test facility and measured data to characterize the performance and robustness of the machine. The paper will conclude with a discussion on lessons learned throughout the course of commissioning and testing. Practical aspects of testing a compressor operating near the dome including complications relating to obtaining an accurate compressor flow map, efficiency calculations, flow unsteadiness, and associated measurement uncertainties will be discussed.

INTRODUCTION

An integrally geared compressor-expander (compander) was developed for use in a nominal 10 MWe concentrated solar power (CSP) supercritical carbon dioxide (sCO_2) plant. The objective of the project was to achieve a target 50% power block efficiency at the design point, and a levelized cost of electricity (LCOE) of 6 ¢/kWh. An integrally geared machine architecture was chosen for its flexibility in incorporating reheating, intercooling, flow control features, and allowing a variety of speeds while maintaining a reasonable CAPEX. The power cycle optimization for the integrally geared compander began with parametric on-design (design point) analysis and concluded with off-design analysis to determine machine performance and controllability at off-design operation. A detailed model of the final integrally geared compander is shown in Figure 1, and the full package in Figure 2; for more details on the project see [1]. The machine comprises four pinions rotating at different speeds. There are two compressor pinions that drive two main compressor stages and two recompressor stages. Additionally, there are two turbine pinions that operate at lower speeds that are powered by four expansion stages. The need for a compressors and re-compressors stems from the selection of a recompression cycle, which provides high performance for applications where the heat source is between 650-700°C. This performance stems from maximizing the recuperation that the cycle supports by eliminating the pinch point in the recuperator in a simple recuperated sCO2 cycle. For the sake of discussion, the main compressor in this study has inlet and outlet temperatures of 35-55°C and 80-100°C respectively, and the recompressor has inlet and outlet temperatures of 84-110°C and 205-215°C.

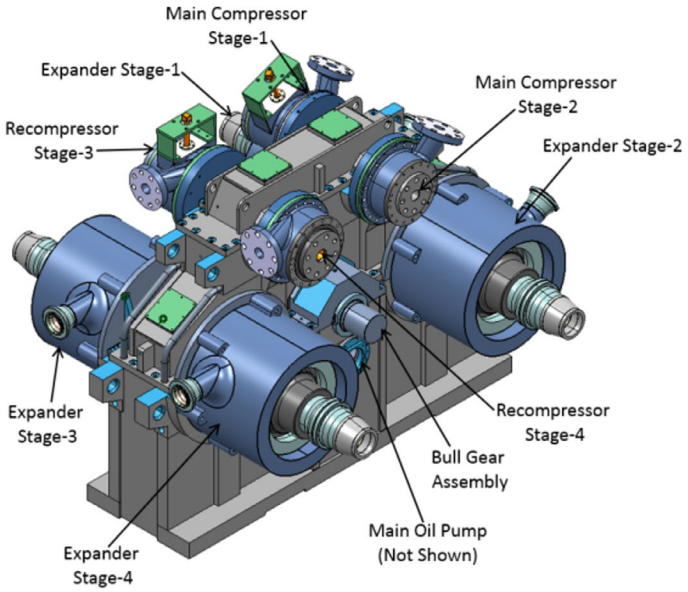

Figure 1. Integrally Geared Compander Turbomachinery Core

Cycle studies were performed in an iterative manner with the System Advisor Model (SAM) [2], developed by National Renewable Energy Laboratory (NREL) to predict the plant economics, and to ensure the selected operation scheme achieved the target efficiency and LCOE [3]. As such, the combination of cycle and SAM studies determined the necessary cycle configuration, which informed the project team of the design conditions for the rest of the equipment.

For the analyses summarized here, the power block efficiency is defined as the ratio of the electrical output work from the generator relative to the heat added to the cycle; thus, it accounts for turbomachinery, recuperator, and generator efficiencies, as well as pressure losses in heat exchangers, piping, and valves. The power required to operate cooling systems was included in the SAM model, and was not included in the power cycle efficiency.

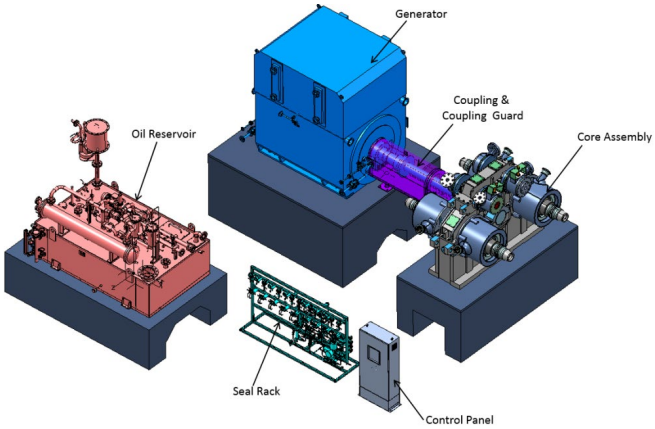

Figure 2. Integrally Geared Compander Package Components

MODEL DEVELOPMENT

Cycle modeling was performed using Numerical Propulsion System Simulation (NPSS) [4], which was linked to National Institute of Standards and Technology (NIST) Reference Fluid Properties (REFPROP) [5] to provide accurate real-gas fluid properties for CO_2. The NPSS cycle was benchmarked against the recompression cycle with intermediate reheat used in [6], and it was found that the predicted cycle efficiencies were within 0.04% of the published values; thus we determined that the modeling technique was acceptable.

ON-DESIGN ANALYSIS

The compander design is unique from in-line machine architectures in that the two main compressor stages, two recompressor stages and four turbine stages are physically separated from one another; thus, inter-stage cooling and reheating can be easily incorporated into the design. A schematic of the cycle with all possible reheat and intercooling configurations initially studied is shown in Figure 3.

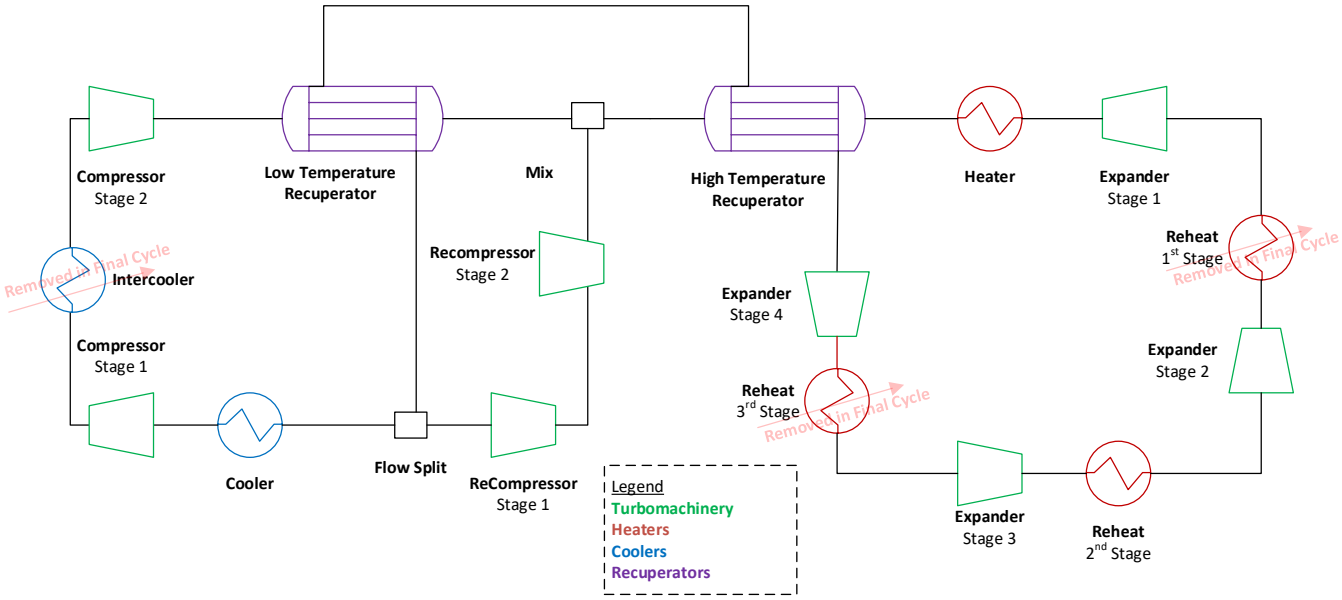

Figure 3. Cycle Schematic Shown with all possible Intercooling and Inter-heating Options

To begin, a literature review was performed to populate pressure limitations for state-of-the-art heat exchangers, recuperators, and piping, and the CO_2 was limited to supercritical operation in all state points of the recompression cycle (i.e. compression and expansion below the dome were not considered). The results of the literature review were combined with turbomachinery efficiency targets based off experience and early 1D stage modeling to develop the cycle model inputs as summarized in Table 1. While this review of literature constrained many facets of the cycle, a number of design choices remained, including (1) the use of intercooling and/or reheating, (2) the selection of cycle pressure ratio, (3) the percentage of flow split between the main compressor and re-compressor, and (4) the off-design control strategy for inventory management and IGV angle. For all cases that use intercooling, the flow is cooled to the same temperature as the primary cooler. Similarly, in all cases that use reheat, the fluid was assumed to be re-heated to the stage 1 turbine inlet temperature (TIT). To determine the optimal configuration of intercooling and reheating to maximize efficiency, eight cycle configurations were simulated at on-design conditions across a variety of flow splits and pressure ratios for a compressor inlet temperature of 55°C. Another factor considered for the intercooling scenarios was the amount of compression handled by the first and second stages. The best efficiencies of this study as a function of pressure ratio are shown in Figure 4.

The results show two groups of curves. The First group shows cycle efficiencies peaking at a pressure ratio of 2.6 for architectures without intercooling; correspondingly the best performer in this group is the case having a single stage of reheat. The second group shows cycle efficiencies increasing with pressure ratio and again, the best efficiency is calculated for the configuration for a single stage of reheat. In both cases, a single stage of reheat increases the efficiency over the other options, with gains due to additional stages of reheat adding little or no benefit. This occurs because the additional pressure drop in the additional reheaters removes the benefit of the added heat. Therefore, from this assessment, we can conclude for further optimizations that we will only consider the case of one stage of reheat before the third stage of expansion, as this maximized efficiency for both intercooled and not intercooled configurations.

To determine whether or not the final machine architecture should incorporate intercooling, the power cycle performance was predicted with compressor inlet temperatures evaluated across the range from 35-55°C for intercooled and non-intercooled designs while pressure ratio and recompression flow split were allowed to float. The best efficiency points for each compressor design-point inlet temperature are shown in Figure 5, which shows generally that efficiencies decrease with increasing compressor inlet temperature, as expected. Additionally, Figure 5 also shows that intercooling requires a higher percentage of flow passing through the recompressor, and that as temperature increases, more pressure ratio is required to maximize gains for the intercooled case, while less pressure ratio is required for the non-intercooled option. Generally, this implies that depending on the atmospheric temperature of your installation site, the configuration for the optimized machine will change. For the present work that used the SunShot vision study (SVS) location [7], an average ambient temperature of 22.0°C with a 15°C approach temperature suggests that a design point temperature of 37.0°C for the compressor inlet is appropriate. At this condition, the configuration without intercooling is the best option, is cheaper, and achieves approximately 50% thermal to electric efficiency at the design point.

Table 1. Cycle Model Inputs

Group	Property	Value
Heat Exchanger	Pressure Drop (each Heat Exchanger)	1%
	High Temp Recuperator Effectiveness	97%
	Minimum Pinch Temperature	5°C (9°F)
	Heater and Reheat Outlet Temperature	705°C (1301°F)
	Cooler and Intercooler Outlet Temperature Range	35-55°C (95-131°F)
Generator and Mechanical Efficiencies	Generator Efficiency	98.7%
	Compressor Mechanical/Pinion Losses	4%
	Turbine Mechanical/Pinion Losses	2%
Pressure Limits	System Min Pressure	73.8 bar (1070 psi)
	System Max Pressure	275.8 bar (1070 psi)
Turbomachinery	Compressor Isentropic Efficiency	83.5%
	Re-Compressor Isentropic Efficiency	84%
	Turbine Isentropic Efficiency	92%

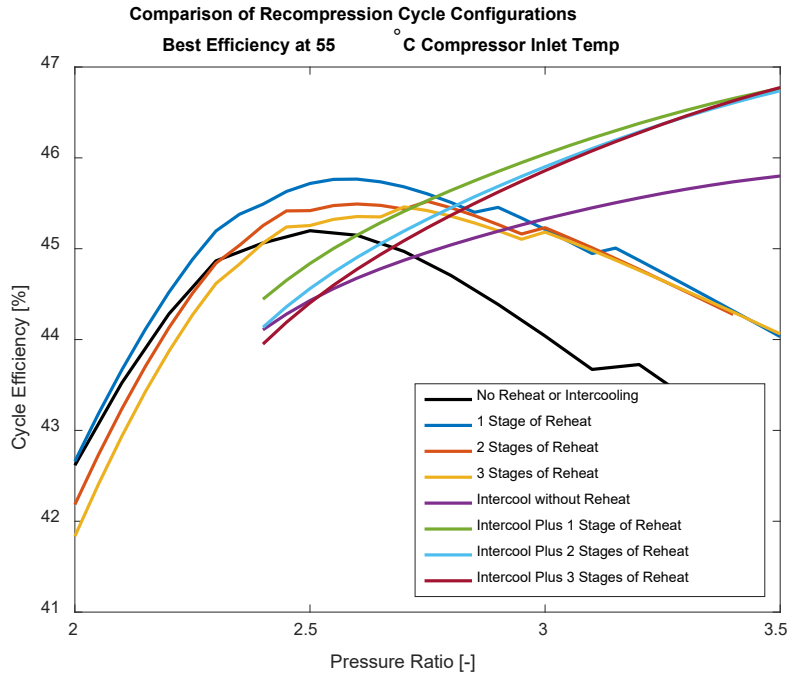

Figure 4. Comparison of Reheat/Intercool Options at 55°C Inlet Temperature

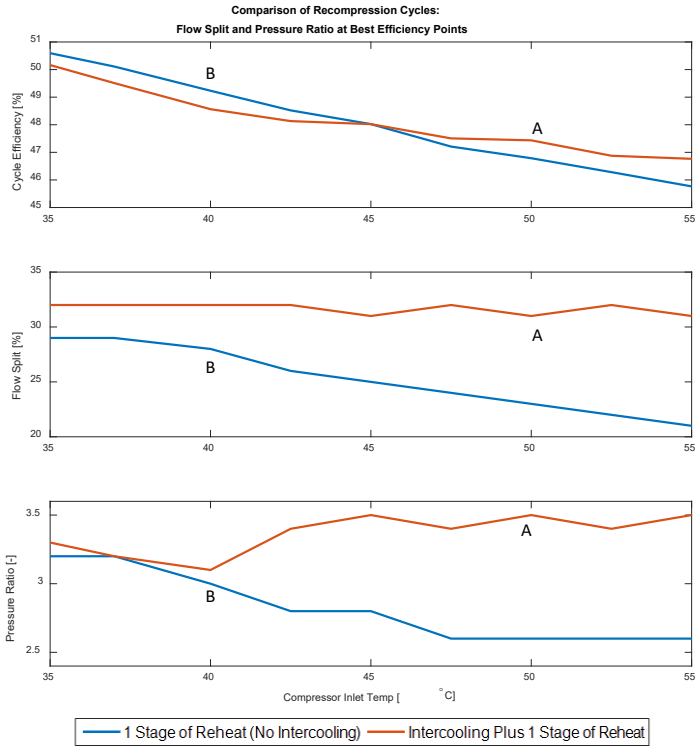

Figure 5. Flow Split and Pressure Ratio of Maximum Efficiency Point against Compressor Inlet Temperature

OFF-DESIGN ANALYSIS

Having selected a machine architecture with one stage of reheat and no intercooling (as denoted by Figure 6), the question remains on how to adequately control the machinery stages to provide maximum efficiency at off-design operation, where the compressor inlet temperature varies due to ambient temperature swings for fixed geometry turbomachinery. While there are a variety of methods that can be used, the approaches typically considered for sCO_2 power cycles include: inventory control (change in system mass/pressure), compressor recycle (hot or cold), and turbine bypass (hot or cold), and flow split through the recompressor. An updated cycle model was developed that included throttle valves for the recycle and bypass control methods and is shown in Figure 6. Initial simulations using this model also included recompressor recycle, but it was found that incorporating recompressor recycle did not improve net power recovery; thus, this control scheme was not investigated further. Heat exchangers were modeled using an effectiveness at design conditions, and recuperator performance at off-design conditions used a Dittus-Boelter-based approach as demonstrated in [8].

One of the key challenges with operating a closed loop sCO_2 Brayton cycle is that cycle efficiency is optimized when the turbine power output is maximized and compressor work input is minimized. For the compressor, this means that it must be operated near the dome where fluid densities are high and viscosity is low. While this may sound trivial, it is challenging to design a machine to operate in a region where the fluid properties change rapidly. Adding to this complexity, a typically solar application is air-cooled, thus the inlet temperature will vary with ambient temperature. To accommodate these changes in inlet temperature, the compressor must be capable of 70% stable operating range while producing a pressure ratio of 2.5-3.5, as depicted in Figure 7. This combination of pressure ratio and range is well outside of the experience of typical centrifugal compressors, as depicted in Figure 8, which is a key challenge in this application. While the expander will see some changes in inlet conditions, CO_2 behaves as an ideal gas in a typical sCO_2 Brayton cycle turbines; thus, it has a less demanding aerodynamic design.

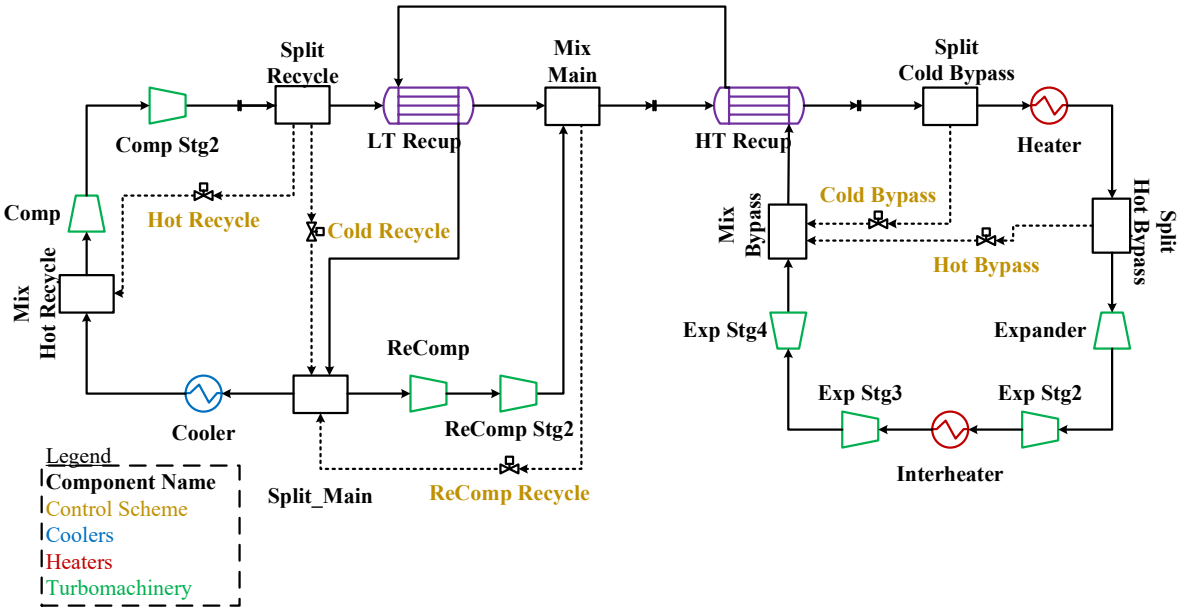

Figure 6. Off-Design Cycle Model

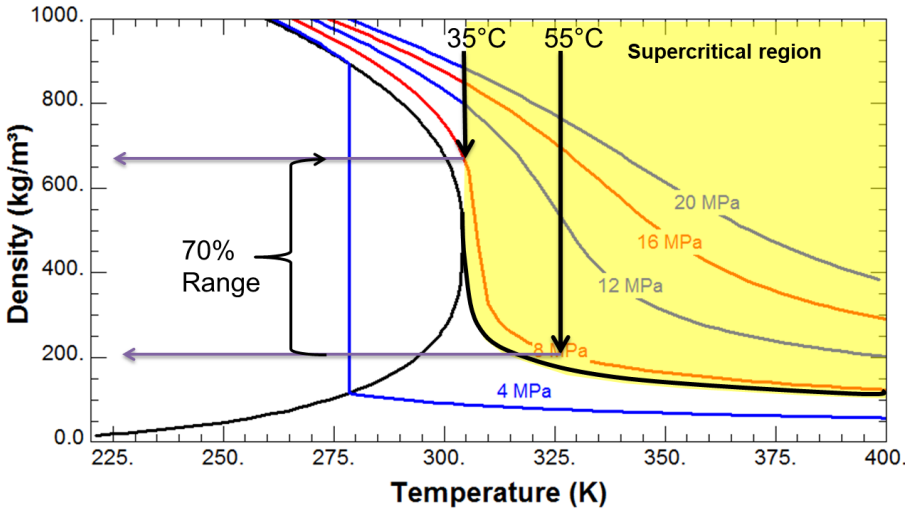

Figure 7. Range Requirement with Changes in Operating Temperature

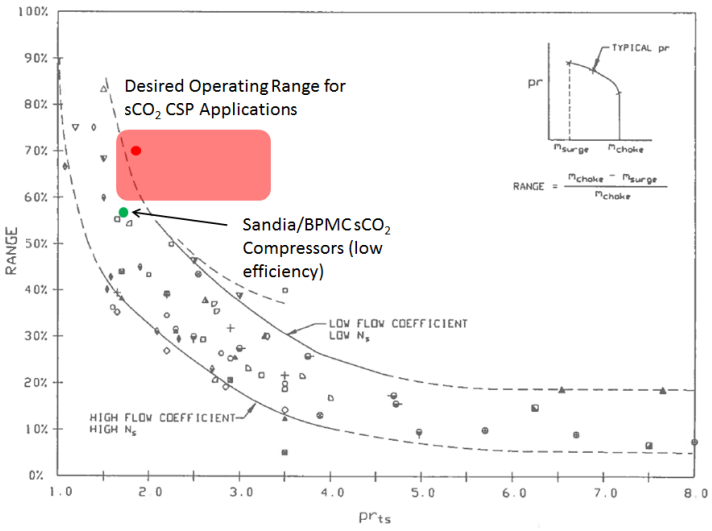

Figure 8. Compressor Experience

In order to compare the relative performance of each off-design control strategy, a parametric study was performed using the range of conditions shown below in Table 2. The best efficiencies as a function of temperature for the various throttle configurations are shown in Figure 9 for one stage of reheat without intercooling. Inventory control and flow split variations were considered for each throttle configuration.

The initial results showed the off-design performance was below on-design performance, even at the design temperature of 37°C. Further investigation found that the best efficiency point of the turbomachinery maps was slightly mismatched from the design point. Better matched turbomachinery maps shift the entire performance curve up, so that on-design and off-design performance are equal at the design temperature of 37°C.

Table 2 – Off-Design Model Inputs

Category	Property	Range of Values
Throttle	Cold Recycle - Main Compressor	1%, 2%, 5%, and 10%
	Hot Recycle - Main Compressor	1%, 2%, 5%, and 10%
	Cold Bypass - Expander	1%, 2%, 5%, and 10%
	Hot Bypass - Expander	1%, 2%, 5%, and 10%
Inventory Control	Mass Flow	-5%,-2%, -1%, 0%, 1%, 2%, 5%, 10%
Recompression Cycle	Flow Split	22% - 32% (1% increments)

The simulation results show that, at temperatures above the design temperature, a combination of inventory control and flow split variation produce higher off-design efficiency compressor recycle or turbine bypass (see “No Recycle” line in Figure 9). Below the design temperature, compressor recycle performs as well as inventory control, flow split, and turbine bypass methods. In general, there is little difference between hot and cold recycle as well as little difference between hot and cold turbine bypass. Compressor recycle helps increase operating range, but it requires additional compression work, which is detrimental. Similarly, turbine bypass improves the range of operation but reduces turbine work. Therefore, compressor recycle and turbine bypass were ineffective relative to other control techniques, leading to the final selection of using inventory control, IGV’s, and flow split to control the cycle during normal operation. It is anticipated that compressor and turbine recycle could potentially be implemented as an emergency control feature, or to improve startup and shutdown; however, this is outside the scope of the current work.

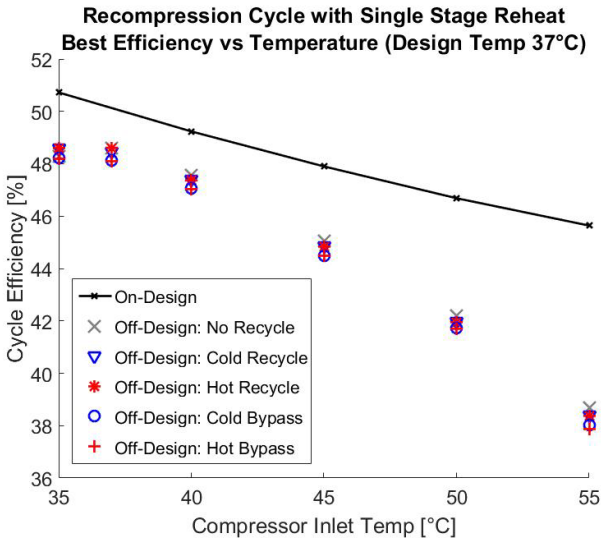

Figure 9. Comparison of Off-Design Cycle Methodologies (All Configurations Include Inventory and Flow Split Control)

The next step performed after the control strategy was selected was to determine the off-design performance of the cycle using a genetic algorithm NSGA-II [9] across a range of ambient temperatures. The genetic algorithm was allowed to vary system mass flow (80% to 120% of design), recompressor flow split (20-34%), and inlet guide vane angles (full range) of the first stage main compressor and first stage recompressor in order to optimize the cycle efficiency. Additionally, the system constraints such as the minimum heat exchanger approach temperature, maximum system pressure, and maximum heat exchanger effectiveness were implemented. It was assumed that the turbine inlet temperature was held constant during all off-design cases.

Off-design predictions focused on two comparisons. The first comparison was of two cycles (one having "Intercool + Reheat," and the other "Reheat Only") having a design point compressor inlet temperature of 35°C. Predicted cycle efficiencies versus temperature for these two cases are shown in Figure 10. Note that the "Reheat Only" produces a higher efficiency throughout the range of compressor inlet temperatures investigated. This notion was presented for cooler compressor inlet temperatures while investigating on-design operation; however, this comparison supports that "Reheat Only" when selecting 37°C as the design point temperature for the turbomachinery is the appropriate configuration for this project when considering the temperature range of expected off-design operation.

The second comparison that was performed was to predict cycle efficiency at off-design for three compressor designs utilizing different design point temperatures for one stage of reheat and no intercooling ("Reheat Only"). The three designs were for compressor inlet temperatures of 35°C, 37°C and 43°C. Figure 11 compares the results of these designs. Each cycle performs best within 2°C of its design temperature, with cycle efficiencies that decrease outside of this range in either direction. Figure 11 shows that the 43°C design temperature performs the best at high temperatures, while the 35°C design temperature performs the best at colder temperatures; therefore, it is necessary to determine where the cycle will operate most often in order to determine which design temperature is best for this particular application. For the current application using the SVS site, the average compressor inlet temperature is 37°C; thus, this design-point temperature was selected as the best balance between efficiency at the design temperature and at off-design. Performing a rigorous investigation of this selection required a technoeconomic analysis. The full discussion of which was performed and discussed in Schmidt et al. [3]. This comparison shows that a design temperature of 37°C reaches a maximum predicted efficiency of 49.8% (within margin of error for 50% goal) and produces higher efficiencies than the 35°C design at higher temperatures.

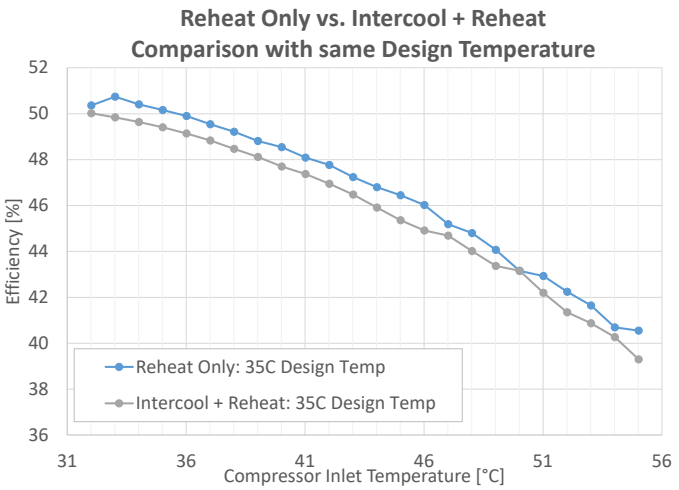

Figure 10. Comparison of "Reheat Only" and "Intercooling + Reheat" at 35°C

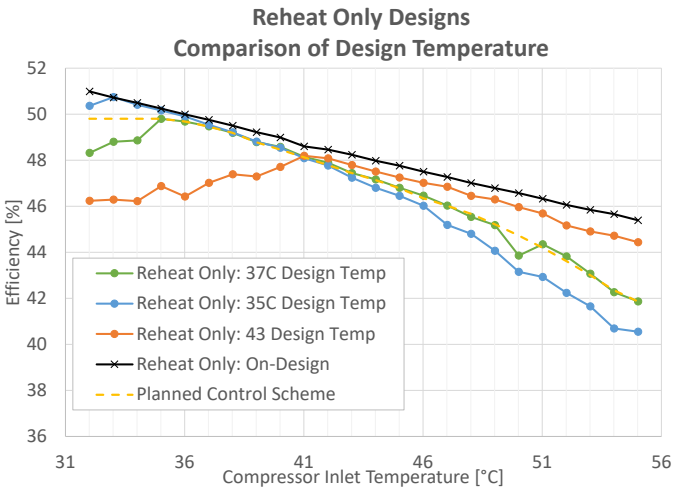

Figure 11. Comparison of "Reheat Only" Cases at 35°C, 37°C, and 43°C

PIPE LOOP DESIGN

While testing the full power cycle was not funded by the current work, the team was funded to perform a compressor test in sCO_2 at full flow, pressure, and speed. This project also supported the testing of the high-pressure high-temperature first stage expander; however, the results discussed here will be limited to the development of the test loop and the performance of the compressor. This test was performed on the full frame gearbox such that the rotordynamics and aerodynamics match the power cycle hardware. See the compander package presented in Figure 12.

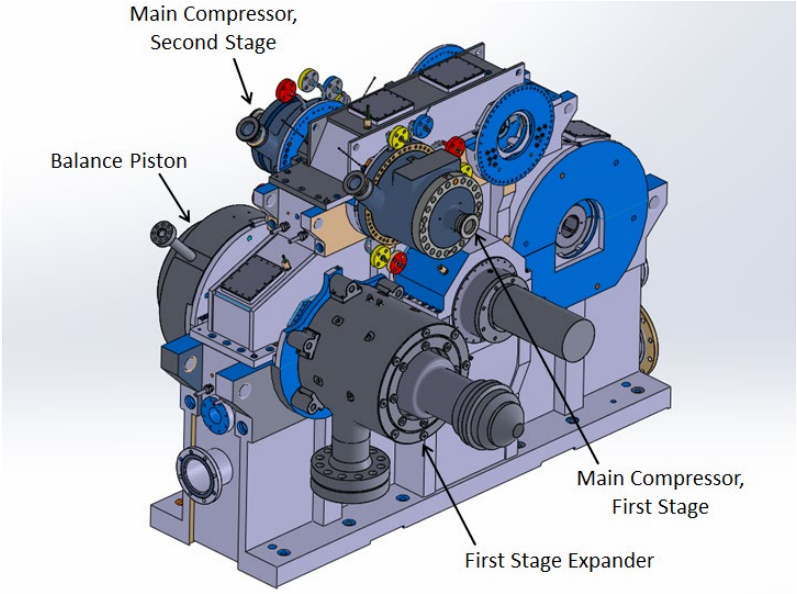

Figure 12. Compressor-Expander (Compander) Package for Component Validation Testing

PIPING LAYOUT & PRELIMINARY SIZING

The integrally-geared compander is designed as a compact and power-dense package. The piping layout was designed to be as compact and simple as possible, while also being easily integrated into the existing machinery facility at the test site, as shown in Figure 13. The process piping was elevated near the compander skid to minimize obstructions for access and to allow ease of access for auxiliary systems such as the dry gas seal supply, lube oil supply, electrical connection, and instrumentation lines. Note that a water-cooled process cooler was installed outside of the lab for ease of access to the water supply and to minimize the potential risk associated with flooding in the event of a pipe failure. All other process piping was located compactly near the compander skid. As a final note, the pipe routing for this test loop was influenced by multiple obstructions in the lab including an existing compressor skid (shown in grey in Figure 13). This compressor skid does not tie into the compander loop; however, its oil supply, process piping, electrical lines, and instrumentation had to be avoided. The piping instrumentation and measurement lengths upstream and downstream of the compressors were based on ASME PTC-10 standards, and included instrumentation at various other critical locations as shown in Figure 14.

Preliminary sizing for each line in the main process loop was determined based off maximum pressure/temperature rating, the expected flow velocity through the line, and the allowable pressure drop for each segment. While this is a compressor test loop and there is room for ample pressure drop, the sizing also must consider the probability for flow induced vibration; thus, velocities were also kept below 30 m/s or less. Pipe sizing was further vetted for the pressure and temperature rating of each section of the cycle, and piping material, diameter, and schedule were adjusted as necessary using ASME B31.3 piping code (2008 version) for carbon steel / stainless steel and ASME B31.1 (2012 version) for Inconel 625 / Inconel 740 as needed. In general, the major pressure losses were limited to below 0.34 bar [.3 bar] for each section, while losses across valve segments were obviously higher. In this case, the frictional losses through the piping were insignificant compared to the predicted pressure drop given the valve flow coefficient (C_v). These calculations were iteratively performed until the system was predicted to perform adequately. This matches the practice that would be used for an installed plant, waste heat recovery system, refinery process, or compressor station with the exception of pressure loss, which would be prioritized higher to avoid reduced cycle efficiencies.

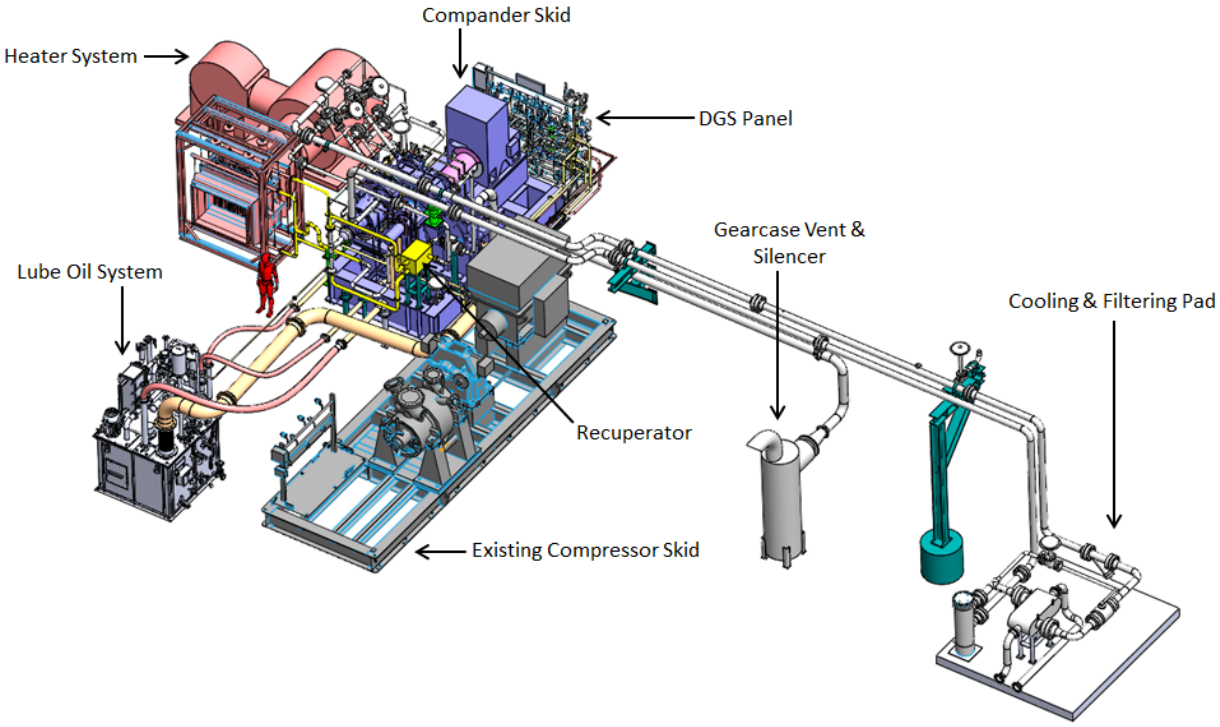

Figure 13. Compander Test Loop Design

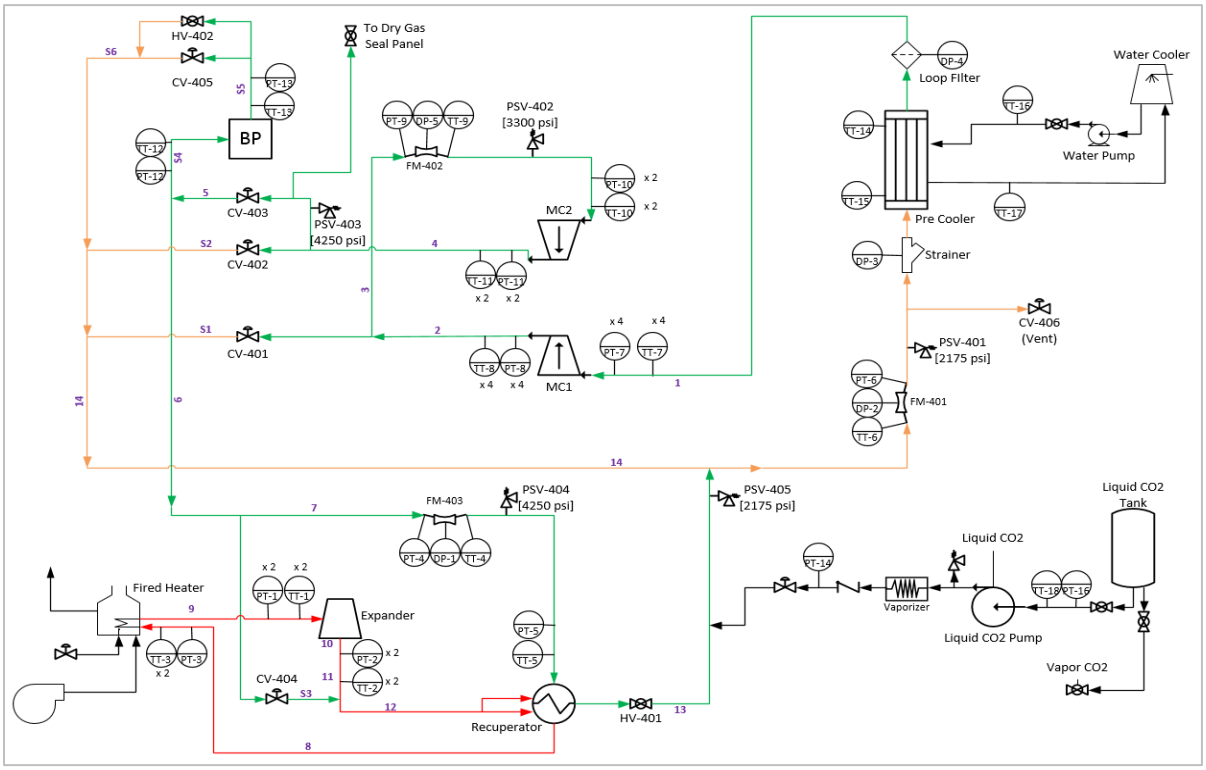

Figure 14. P&ID for Reduced Flow Test Loop

Pipe Thermal Evaluation

The piping system was analyzed in Caesar II thermal pipeline modeler (1) to predict piping stress and displacement due to weight, pressure, and thermal growth; (2) to calculate the nozzle loads on the compander compressors and expander, heat

exchangers, and heaters; and (3) to calculate the modal frequencies of the piping system. The layout of the piping, position of concentrated masses, and the support system design (including support locations and types) were adjusted iteratively to minimize the nozzle loads on the equipment and limit piping stresses to meet code allowables (based on ASME B31.1). Minimizing nozzle loads on an integrally geared machine is critical, as National Electrical Manufacturers Association (NEMA) nozzle loads for integrally geared machines are generally lower than for a barrel style compressor.

While the bulk of the loop was constructed using A312 TP316L Stainless Steel, A106 Grade B Carbon Steel, Inconel 625, and Inconel 740 were also utilized. Reducers and tees were defined where appropriate, and process control valves and hand valves were included in the piping model at the appropriate locations, with manufacturer-specified lengths and weights. Rigid weights were also included in the model for the flange pairs (including flange pairs for piping spool breaks). Preliminary piping support locations were chosen based on the available spacing near the compander skid, and supports were modeled primarily as weight supports with a small amount of stiffness in the lateral and axial directions. Three temperature cases were defined for each line – hot case, operating case, and cold case to consider conditions where the turbine was hot or cold. Using the three temperature cases defined above, twelve load cases were analyzed to determine the acceptability of the piping system. All nozzle loads, pipe constraint forces, and pipe criteria per B31.1 were adequately met by the model.

After several iterations to the piping design in Caesar II, it was evident that the allowable equipment nozzle loads were the limiting factor in this test loop design. The thermal stresses were passing the ASME B31.1 code allowables with minimal modifications; however, multiple design iterations were required to meet the limited nozzle load capacity on the compressors. Since nozzle loads deflect the casings on integrally geared machinery relative to the gearbox where the pinion is supported, this deflection has the potential to cause rotor-to-stator rubs in the turbomachinery. Several of the standard weight supports were replaced with spring hangers to provide consistent weight support while allowing for thermal growth away from the compander. The quantity and location of the spring hanger supports on the elevated piping were iterated to minimize nozzle loading.

In addition to the support types and locations, design iterations on the pipe routing and the location of concentrated masses (valves, flanges, etc.) were required to unload the compressor nozzles. The final design iteration balances the weight distribution across the supports such that the compressor nozzles remain unloaded during hot operation, standby, and cold ambient conditions. The final piping system design is considered stable, in that small changes in the location of concentrated masses, support locations, and piping lengths do not significantly alter the compressor nozzle loads. The robustness of this design is consistent with typical practice for a power plant or compressor station, and operation has produced no unexpected consequences at full-pressure and full-temperature operation.

Energy Institute Vibration Screening

Using Caesar II, the lowest mechanical natural frequency (MNF) in the piping system was predicted at 2.1 Hz. Generally, the team recommends that all MNFs in the main process piping should be above 15 Hz to minimize vibration risk. For this test loop, 39 modes were predicted below 15 Hz. Because the low nozzle load allowables on the compressors were the primary driver in the piping design, stiffening the system to increase the lowest MNF above 15 Hz was not practical.

In order to minimize the risk of piping vibrations, the Energy Institute (EI) guideline for avoidance of vibration induced fatigue failure in process pipework was applied. This guideline considers the velocity, viscosity, and density of the process fluid as a measure of how much excitation energy is present. This is coupled with the lowest MNF of each section of pipe to determine a likelihood of failure (LOF) factor. Note that “failure” is referring to the presence of vibrations and not necessarily a fatigue failure in the piping. Specific actions were then taking on pipe sections where the LOF > 0.5.

After application, this guideline led us to increase line size on several sections of the pipe to reduce the local fluid velocities and excitation energy. The majority of the piping sections had a predicted LOF below 0.5, meaning no further modifications are required. For the remaining sections, the lines were monitored during startup and operation for excessive vibrations. No corrective action was necessary. Figure 15 shows some photos of the completed test facility.

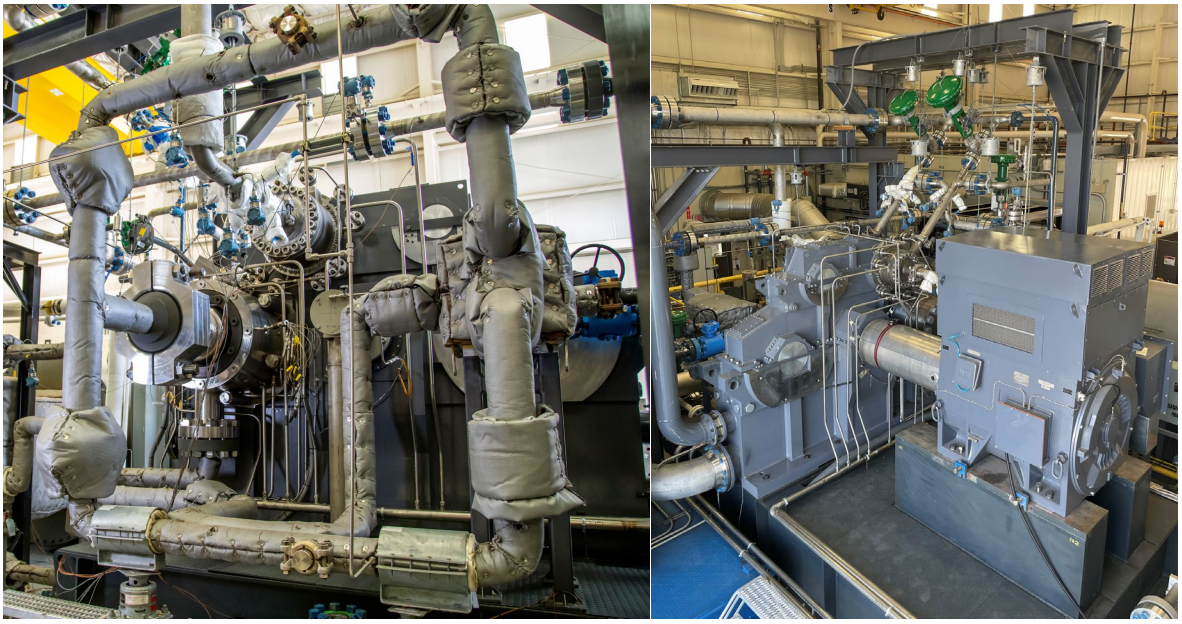

Figure 15. Completed Test Loop

COMPRESSOR DESIGN

The compressor used in this test was designed to match the main compressor specification in Table 3 below, and developed for operation near the critical point in sCO2. The impeller is a semi-shrouded centrifugal stage, with a low solidity vaned diffuser and volute. A multi-step labyrinth seal is used at the eye where the shroud begins. A self-recirculating casing treatment was adapted over the unshrouded axial inducer portion of the stage. This was applied to increase stable operating range and mitigate the effects of pressure fluctuations due to the onset of stall. The impeller was sized at a design point of 37degC and 85.2BarA. Further details of the aerodynamic design are located in [10], the mechanical design [11], and testing in air [12] were reported previously. High fidelity CFD modeling to evaluate the potential for local multi-phase flow development was completed prior to testing and reported [10].

The impeller was manufactured in titanium using 3D printing. Surface finish was refined using an extrude hone process to ensure that the maximum roughness in the blade passages did not exceed a Ra of 3.2µm. The finished compressor impeller is shown below in Figure 16 (left), and a cross-section of the test configuration is shown in Figure 16 (right).

Table 3: Turbomachinery Design Parameters.

Parameter	Units	Compressors		Expanders
		Main	Re-Comp	
Mass Flow rate	kg/s (lb/s)	55.0 (121.25)	22.5 9 (49.5)	77.5 (170.5)
Inlet Pressure	barA (psia)	85.2 (1235)	86.0 (1247)	264.0 (3829)
Inlet Temperature	degC (degF)	37.0 (98.6)	91.9 (197.4)	705.0 (1301)
Discharge Pressure	barA (psi)	272.5 (3945)	269.8 (3916)	89.0 (1291)
Power	kW (HP)	1989.4 (2704)	1961.0 (2666)	13982.0 (19010)

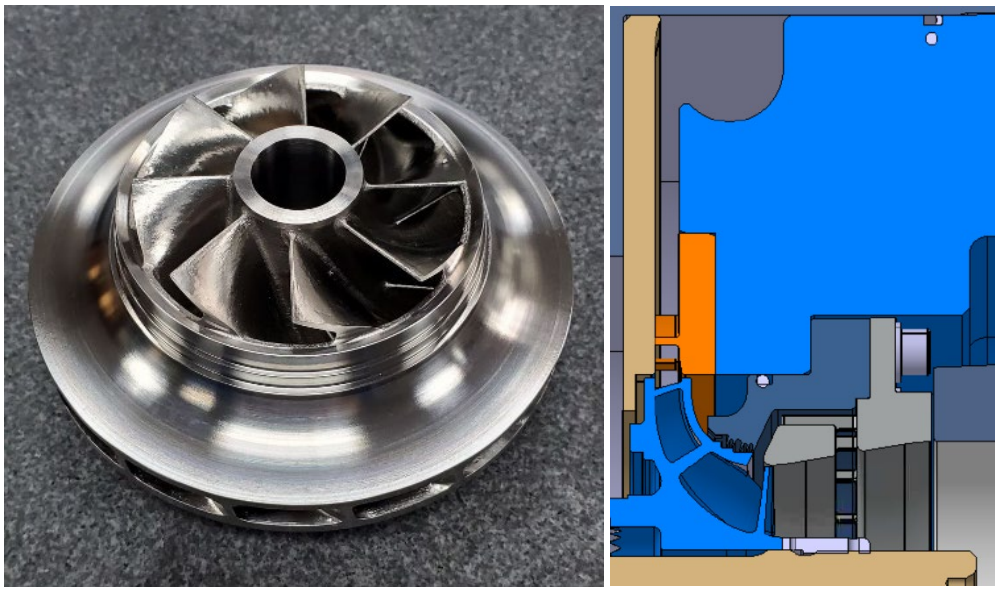

Figure 16: Compressor Impeller (left) and Compressor Test Geometry (right)

CORE DESIGN

The core of the gearbox was constructed to be a nominally 10 MW class electric output; however, the gearbox should support integrally geared sCO_2 companders with power outputs as high as 25 MWe. The fabricated structural steel gearbox has an approximate dimensional envelope of 3.2m x 1.2m x 2.7m, and can accommodate four pinions. The gearbox housing (case) has a three-piece construction: the lower, upper and top case. For the full recompression cycle for concentrated solar power applications, two compressor pinions would be mounted in the split lines between the upper and top gear cases, while two expander pinions would be mounted between the lower and upper gear cases as shown in Figure 1. For the purposes of this testing program, only two of the pinion shafts were used. One pinion has the two main compressor stages, while the second pinion on the lower case has one expander stage on the non-drive end, and a balance piston on the drive end. Both the upper and top cases are designed with oil drain cavities aligning with cavities in the lower case for rapid draining of oil from the side drain port of the gear box through a pipe to the lube oil reservoir. The gear box is designed to minimize the windage losses, and most of the bearing oil drains through lateral internal cavities that by-pass the main bull gear chamber and lead directly to the drain port. Figure 17 shows an axial view of the gearbox housing at the assembly facility while Figures 18 and 19 show the bull gear and pinion, respectively.

Figure 17. Gear Box Housing Axial View

Figure 18. a) Bull Gear, b) Bull Gear and Expander Pinion Assembled in Gearcase

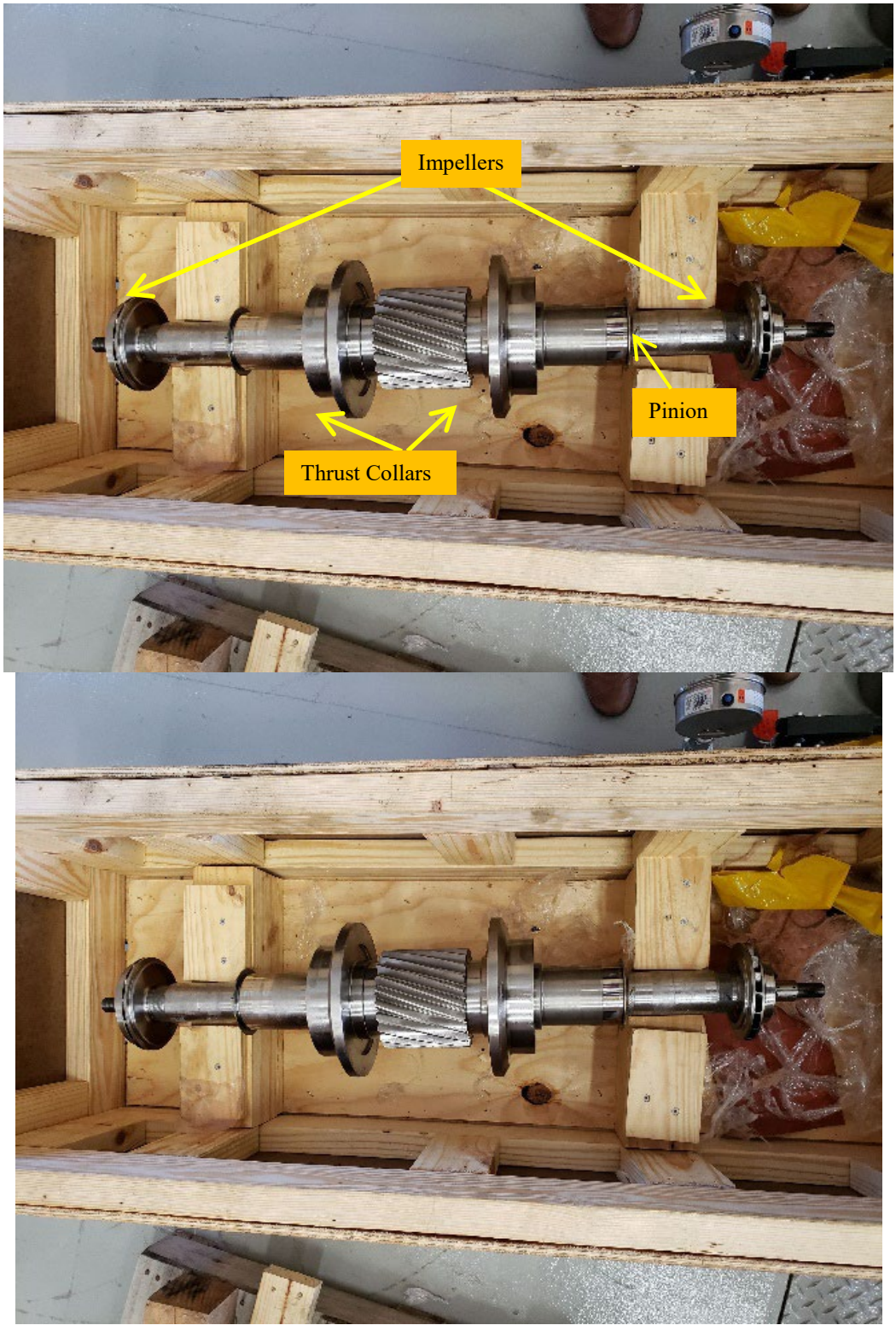

Figure 19. Compressor Pinion shaft with Thrust Collars and Impellers Mounted

Rotordynamic Design

One challenge of high-speed turbomachinery is avoiding unstable vibrations in the pinion and bull gear during operation. API 617 and 684 define the mechanical acceptance criteria for the pinion and bull gear rotor dynamics. The analysis was conducted by using the software package XLTRC2 developed by Texas A&M University.

Operation in sCO2 leads to some unique rotordynamic challenges, since the dense fluid can create large destabilizing forces on the pinion. These cross-coupling forces are particularly difficult to manage for a pinion with a first natural frequency that is below the running speed. A sub-critical pinion, with a 1st natural frequency above the running speed, is dynamically very robust and usually cannot be destabilized by the fluid cross-coupling. Great efforts were spent to develop a sub-critical compressor pinion, including optimizing the shaft geometry, the bearing design and the impeller mass. Figure 20 (left) below on the left shows the mass-elastic lateral model of the main compressor pinion. Figure 20 (right) below on the right shows the unbalance response plot at the non-drive end bearing location. Per API 617 and 684, the magnitude of the unbalance is four times the value of U, as calculated by U=6350 (W/N), where W is the rotor mass and N is the pinion speed. The pinion operates at 27,572 rpm and the first natural frequency was calculated to be 36,670 CPM giving a separation margin of 33%, which satisfies the API required 25% separation margin.

Finally, a Level II API stability analysis was conducted. The analysis calculated the first forward mode to have a logarithmic decrement (log dec) of 1.55 and the second forward mode has a log dec of 0.21. All the modes met the API stability requirements of 0.1.

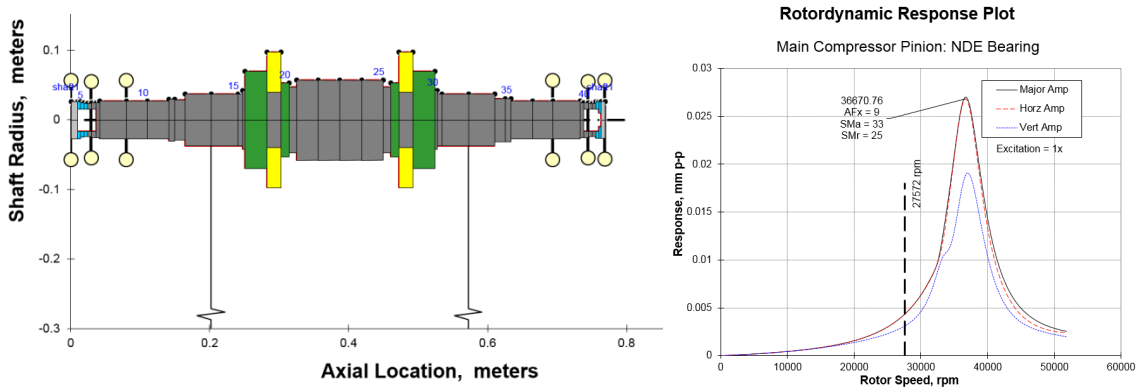

Figure 20: Main Compressor Mass-elastic Lateral Model (left) and Unbalance Response Plot at the Non-drive End (right)

Seal Selection

Unlike steam turbines that have a sub-atmospheric pressure on the low-pressure side of the machine that requires water as makeup, the sealing pressure for sCO2 systems in this machine ranges from 83-255 bar. Since CO_2 at these pressures has high density and low viscosity, leakage mass flow can be large and costly. Investigating the technoeconomics of supplying makeup gas, utilizing dry-gas seals (DGSs) is the only good option for an integrally geared machine. Other machine architectures have proposed carbon ring seals or hermetic casings, but neither of those options are viable for compander architectures. The compander developed during this program utilized a tandem DGS on both the compressor and turbine pinions. Tandem DGSs allow for the primary seal leakage to be reclaimed and pressurized back up to suction pressure using a reclamation system. Tandem DGSs add shaft length, which complicates rotordynamics; however, looking at Figure 19 it can be observed that in comparison to atmospheric integrally geared machines, the impeller is relatively small in comparison to the pinion. This in conjunction with large shaft diameters required to transmit the high torques inevitable on sCO2 machines, makes subcritical operation possible. This was the case for this compressor pinion, which operates approximately 15-20 percent below its critical speed.

Gearing

Involute profile helical gears were chosen as is typical for high-speed gearing applications to ensure smoothness of engagement. The gear design analysis was performed per AGMA 2001-D4 and AGMA 925-A03. The minimum factor of safety achieved was 1.96 and the maximum scuffing probability was 8.8%. The bull gear and the pinion shafts are made of high strength normalized low/medium carbon alloy steels (Grade 2 material), and the gear teeth are case carburized to provide adequate strength and wear resistance.

Table 4. Basic Gear Design Input Parameters.

	Bull Gear	Expander Pinion 1	Expander Pinion 2	Compressor Pinion 1	Compressor Pinion 2
Shaft speed, rpm	1800	17331	14795	27573	28886
Rated power, kW		6580	7402	2053	2052
Strength minimum Safety factor	1.6				
Scuffing maximum permissible probability *(per AGMA 925-A03)*	10%				
Life rating (AGMA 6011), hrs	175,316				
Gear Service Factor) per API 617	0.80				

Thrust Collar

For the pinion thrust collar design shown in Figure 21, the design, choke and stall conditions were checked to take into account the maximum load on the collars. In addition, the press fit of the collars on the shaft was checked for the maximum temperature differential and interference relaxation due to centrifugal growth. In both cases, the design safety factor achieved for the thrust collar fit was greater than 10, assuring design adequacy.

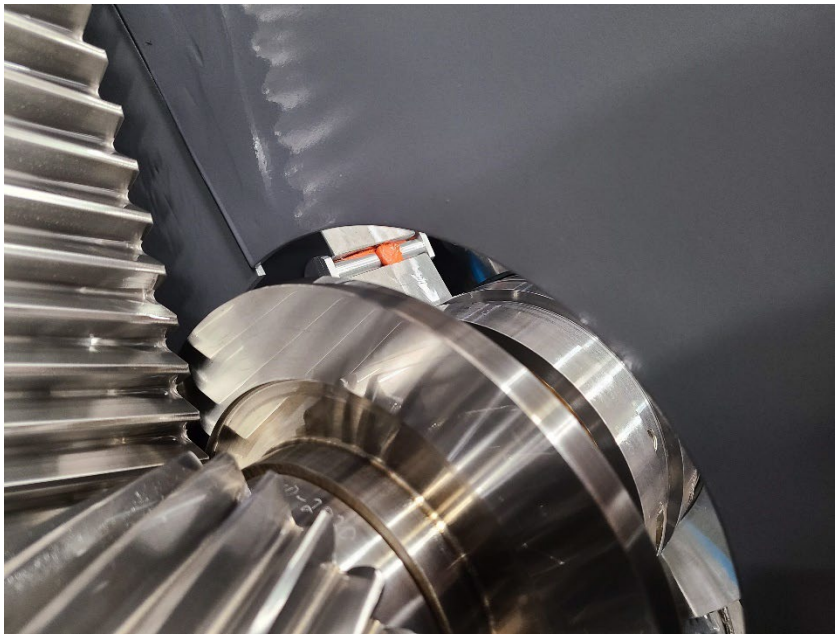

Figure 21. View of Thrust Collar on Pinion.

Lubrication

The gearbox utilizes ISO VG 46 lubrication oil that is supplied by a main oil pump mounted on the non-drive end of the lower case of the gearbox coupled to the bull gear. This allows easy service and replacement of the pump without disturbing other components. A common oil inlet supplies oil to lubricate all the gears and bearings through internally machined passageways. The design overall oil flow rate for the 10 MW design is 1450 l/min. The gears are lubricated by oil injection using an in-mesh and out-mesh lubrication system through internal machined ports and spray nozzles.

The in-mesh lubrication is used for gears and thrust collar lubrication, and out-mesh is used mainly for cooling the gears. A vacuum blower and demister is installed in the oil reservoir vent line to create a vacuum to minimize windage, help prevent leaks, and reduce oil-mist issues. The gearbox frame also includes oil passages to provide adequate oil at the top oil nozzle ports for the lubrication and cooling of the gears, while deflectors are added to the gearcase to divert the oil towards the bottom of the gearbox to reduce entrainment and splashing of the oil and reduce overall windage losses.

Core Instrumentation

Instruments like RTDs, key phasor and position sensors are supported inside of the gearbox, with wires routed securely to keep them away from the rotating parts. Each pinion has a key phasor and axial position probes on the thrust collars. In addition, bearing and dry-gas seal instrumentation wiring is routed through dedicated passages within the sealed split lines of the gearbox.

Mechanical Efficiency Performance

A flow meter and temperature probes were installed in the lube oil supply system so that the heat loss though the oil could be measured. The heat transmitted to the oil is a good measure of the mechanical losses of the system. The mechanical power was calculated based on the measured flow of oil into the core and temperature rise of the oil from inlet to outlet of the gearbox. Heat loss to ambient was not accounted for, but is estimated to be less than 5% of the overall heat loss of the system. The measured mechanical losses matched closely with the design prediction. Additionally, the mechanical losses were found to be nearly constant at 100% speed and closely matched design expectation.

PERFORMANCE

While other works will focus on the overall testing of the compander in a loaded turbine configuration, the results presented here will focus exclusively on the performance of the compressor pinion and bull gear. For this test, only one compressor pinion was operational in the machine. The other pinions were removed, and the bearing ports were plugged with blanks.

Bull Gear – Vibration

The bull gear rotor bearings were designed with large load-carrying capacity and a very stable log dec, larger than 2 for the 1st and 2nd modes, and no exictation peaks were expected within operating speed range. Figure 22 shows the bull gear synchoronous vibration during coast-down; the vibration level stays below 10um and is stable, as expected. Figure 23 shows the FFT of the bull gear rotor at full speed. About 5um synchronous vibration is observed on the plot at 30 Hz, which aligns with analysis predictions. There are some components at 2X, 3X, 4X and 5X running speed on the FFT output, which could be due to the interaction within the IGC rotor system or potentially from mechanical run-out (scratches) on the probe track areas, but they do not have any impact on the rotor stability.

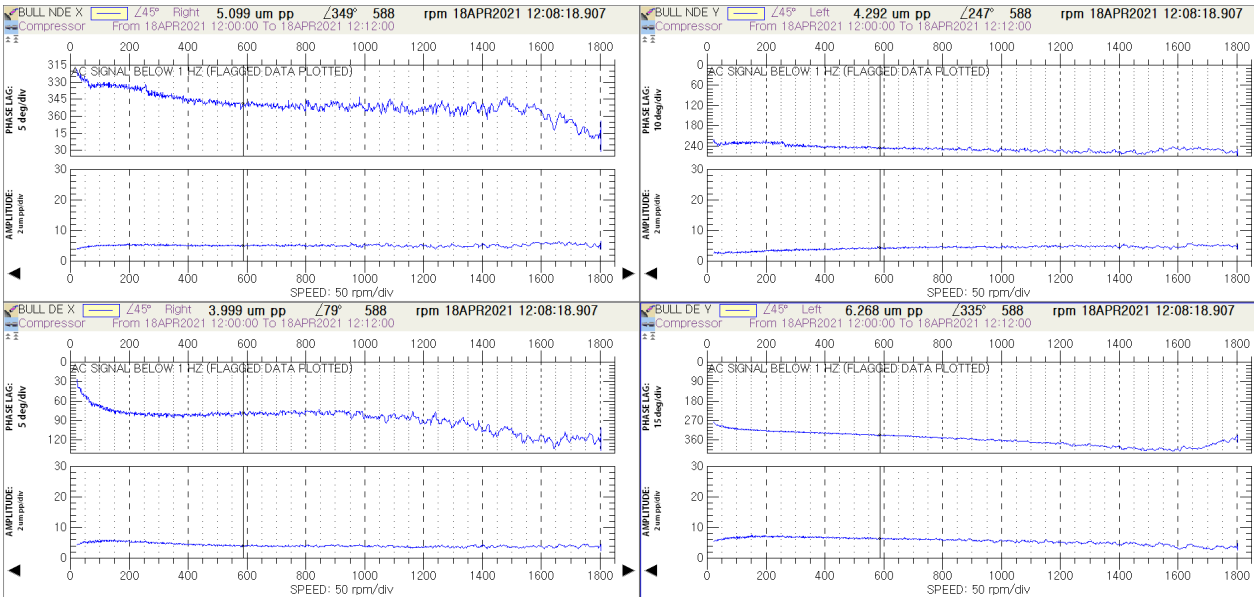

Figure 22. Bull Gear Shaft Synchronous Coast-Down Vibration

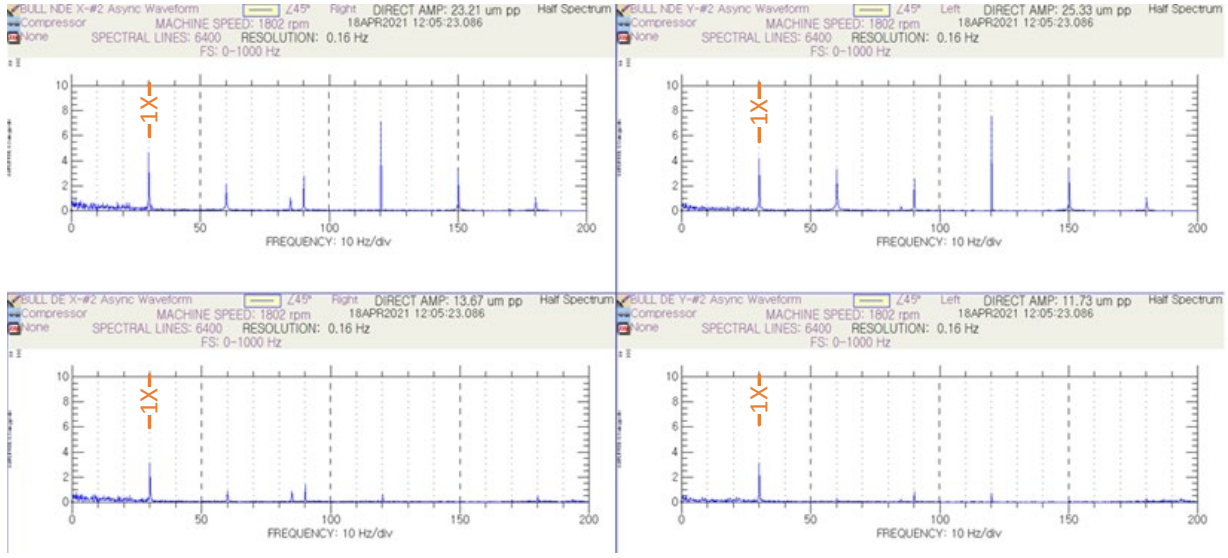

Figure 23. Bull Gear Shaft FFT at Full Speed at 83 barA

Compressor-Vibration

The compressor rotor is designed to be subcritical. i.e. it operates below all critical speeds. With all the critical speeds above the operating speed, the rotor-bearing system is not susceptible to classical aerodynamically induced cross-coupled instability having whirl frequency ratios at approximately 0.5. Figure 24 shows the compressor rotor synchoronous vibarion during coast-down, and the vibration level stays below 12um and is stable. Figure 25 shows the FFT of the compressor rotor at full speed. Synchronous vibration at 422Hz was very low at the 1st stg and around 5um at the 2nd stg, which are dependent on residual unbalance and bearing load. Relatively large components at turbine operating speed can be observed from the FFT plot, which indicates cross-talk of turbine rotor vibration being transferred through the bull-gear. The pinion cross talk between the turbine and compressor has no impact on the compressor rotor stablity. The test demonstrates that the compressor rotordynamic design meets API-617 vibration limits.

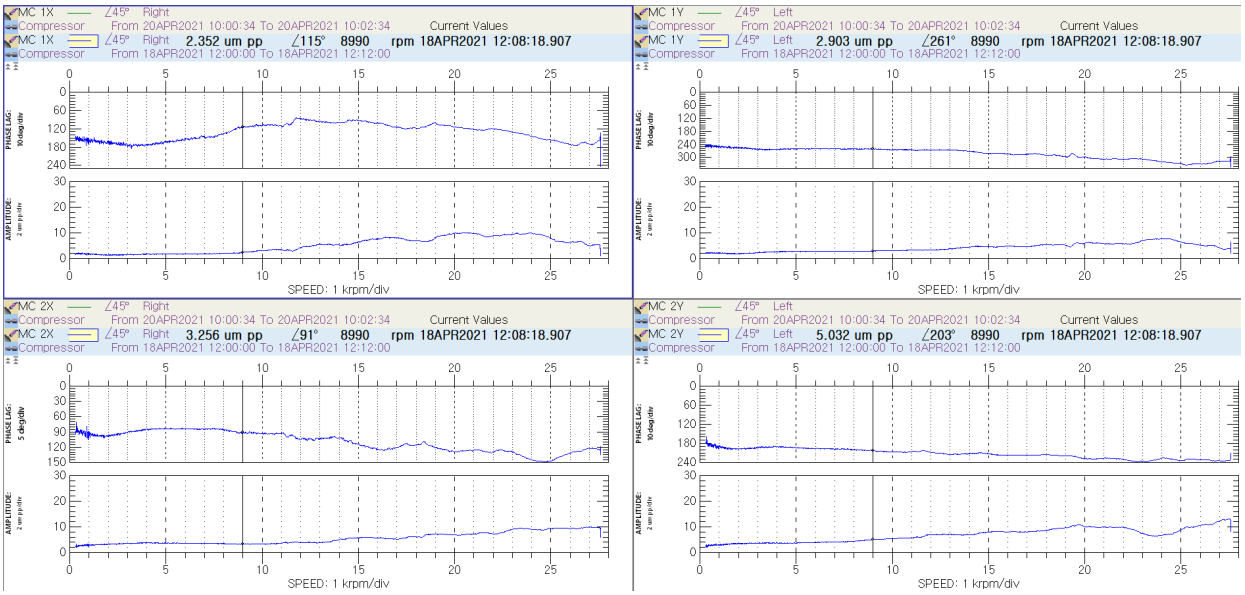

Figure 24. Compressor 1 and 2 Shaft Synchronous Coast-Down Vibration

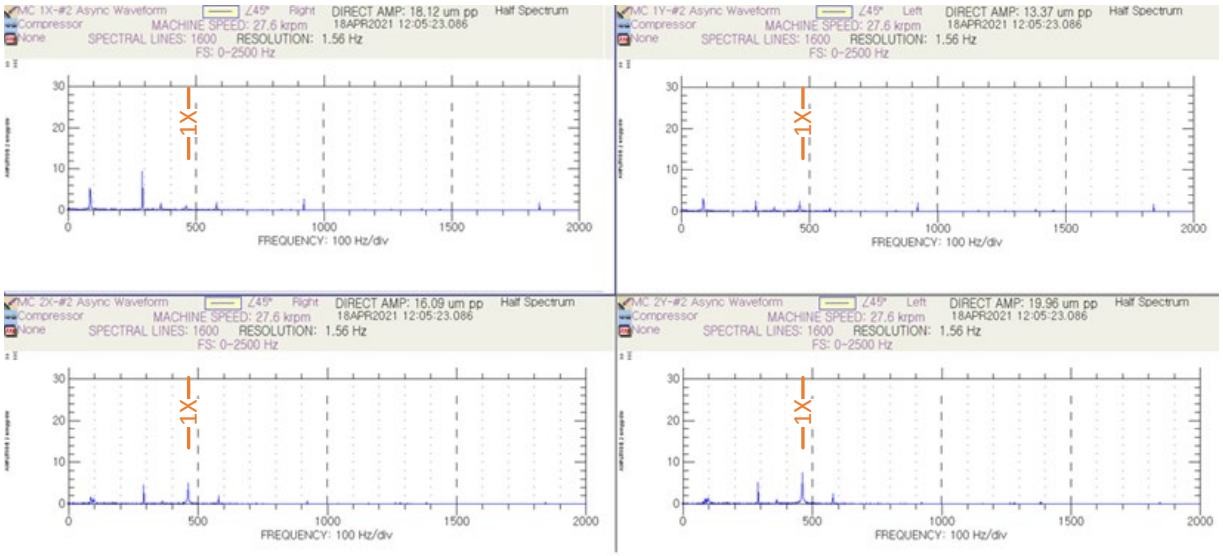

Figure 25. Compressor 1 and 2 Shaft FFT at Full Speed at 83 barA

Bull Gear Bearings

The bull gear is designed to handle large and various directional loads by using tilting pad bearings at 270mm journal diameter. The bull-gear thrust bearing is designed to handle up to 150kN thrust load. Figure 26 shows the bull gear journal and thrust bearing temperatures for a typical run. The maximum temperature of the journal bearings at full operating speed is about 77°C (170.6°F), which is what was predicted by the analysis. The thrust bearing temperatures were well below the allowable limits because the test thrust loads are much lower than the designed load capacity.

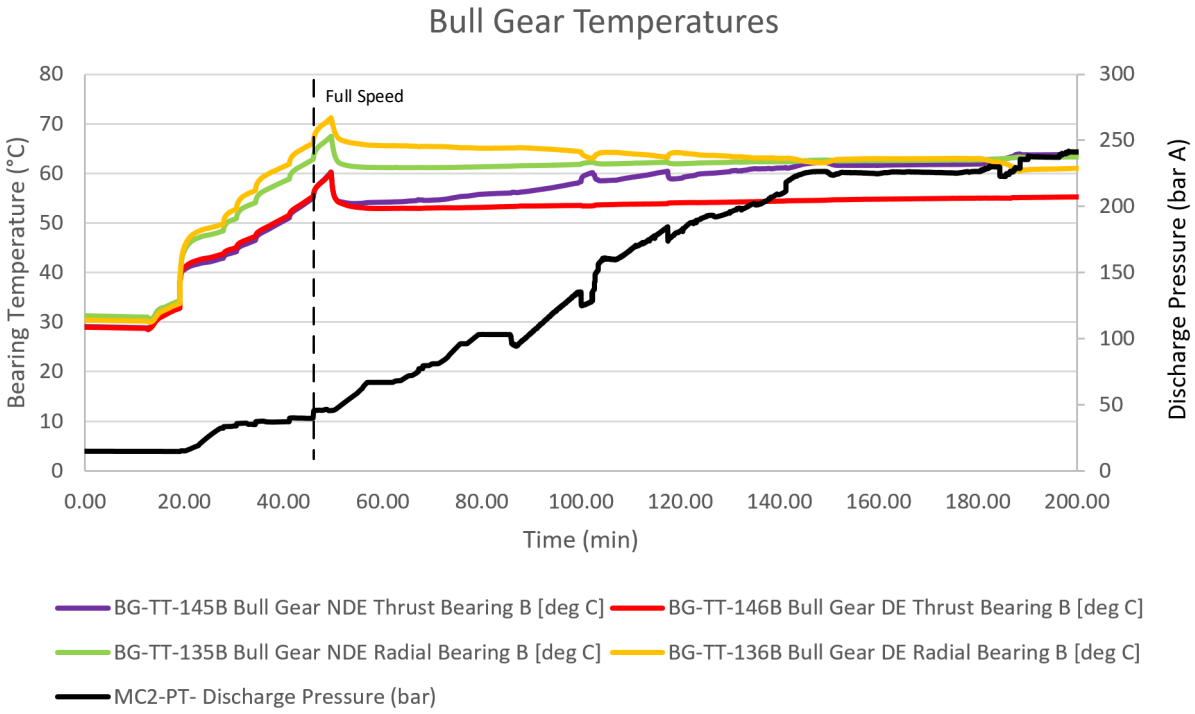

Figure 26. Plot of Bull-Gear Bearing Temperatures During a Three-Hour Test

Compressor Bearings

The compressor bearings are designed to be a load between pad configuration at worst case load conditions. Also, a pivot offset for the pads of 0.6 is applied, which can help reduce the bearing temperature. Figure 27 shows the compressor bearing temperatures at various speeds. The maximum temperature of the journal bearings at full operating speed is about 88°C (190°F), which was predicted by the analysis. The lube oil supply temperature is regulated with a thermostatic valve and typically reaches about 49-54.5°C (120-130 °F).

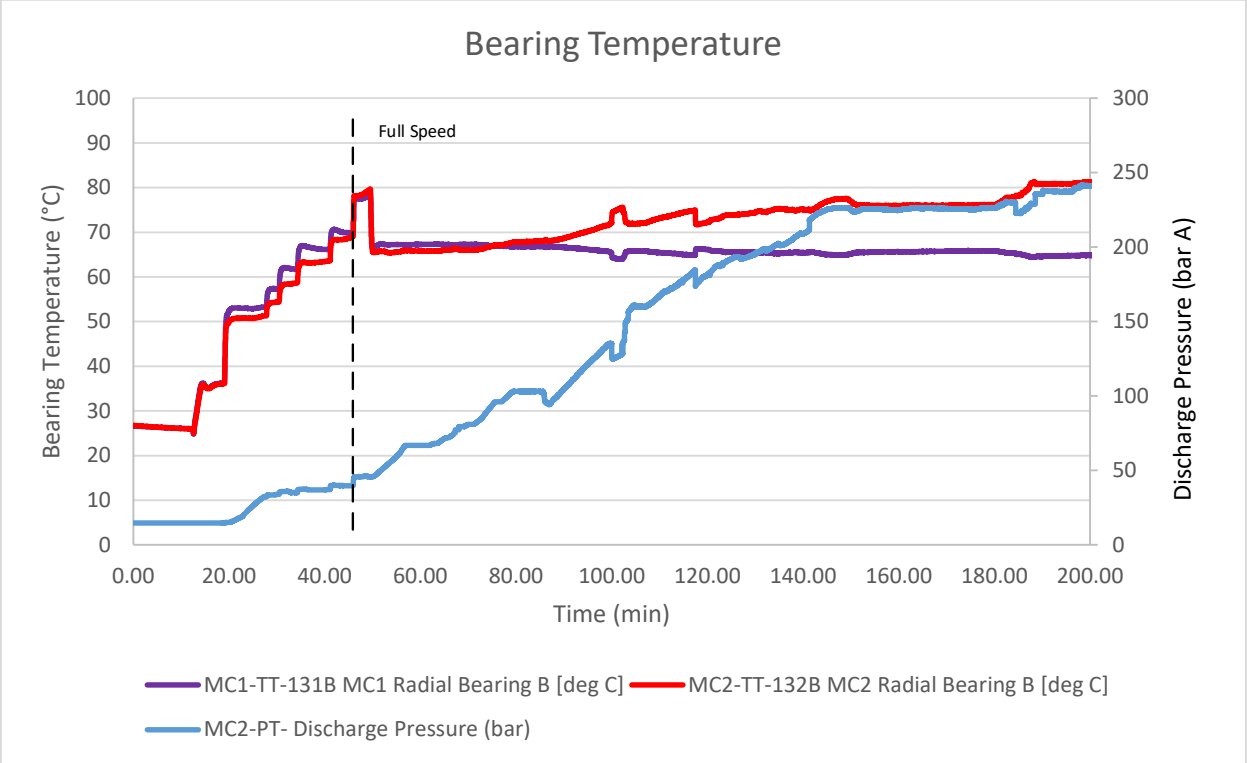

Figure 27. Plot of Compressor Journal Bearing Temperatures During a Three-Hour Test

Table 5 below summarizes the bearing temperature and overall vibration including synchronous and nonsynchronous vibrations. All the numbers are well below the alarm level, indicating successful design of all the rotors and bearings.

Table 5. Bearing Temperatures

Apollo	Limit	Alarm	Actual
BG Thrust Bearing Temp °C (°F)	120 (248)	110 (230)	78 (172.4)
BG Journal Bearing Temp NDE °C (°F)	120 (248)	110 (230)	62 (143.6)
BG Journal Bearing Temp DE °C (°F)	120 (248)	110 (230)	71 (160)
Comp Bearing Temp NDE °C (°F)	120 (248)	110 (230)	82 (179.6)
Comp Bearing Temp DE °C (°F)	120 (248)	110 (230)	80 (176)
BG Vibration NDE µm (mils)	100 (3.93)	70 (2.76)	29 (1.14)
BG Vibration DE µm (mils)	100 (3.93)	70 (2.76)	19
Comp Vibration NDE µm (mils)	42 (1.65)	29.5 (1.16)	26.3 (1.04)
Comp Vibration DE µm (mils)	42 (1.65)	29.5 (1.16)	26.4 (1.04)

Dry-Gas Seal Performance

Figures 28 and 29 show the internal DGS temperatures recorded during a three-hour run on the machine up to a discharge pressure of 250 bar. In general, it can be observed that the DGSs increase in temperature with speed and pressure up to approximately a 60-80 bar discharge pressure, then the seals start to cool down with further increases. This change is because the leakage across the seal begins dramatically increase as the seals become supercritical,

increasing the effectiveness of the cooling on the DGS. It should be noted that during this test, the DGS stream was not heated, as windage in the DGS was sufficient to prevent the formation and accumulation of dry ice in the discharge stream.

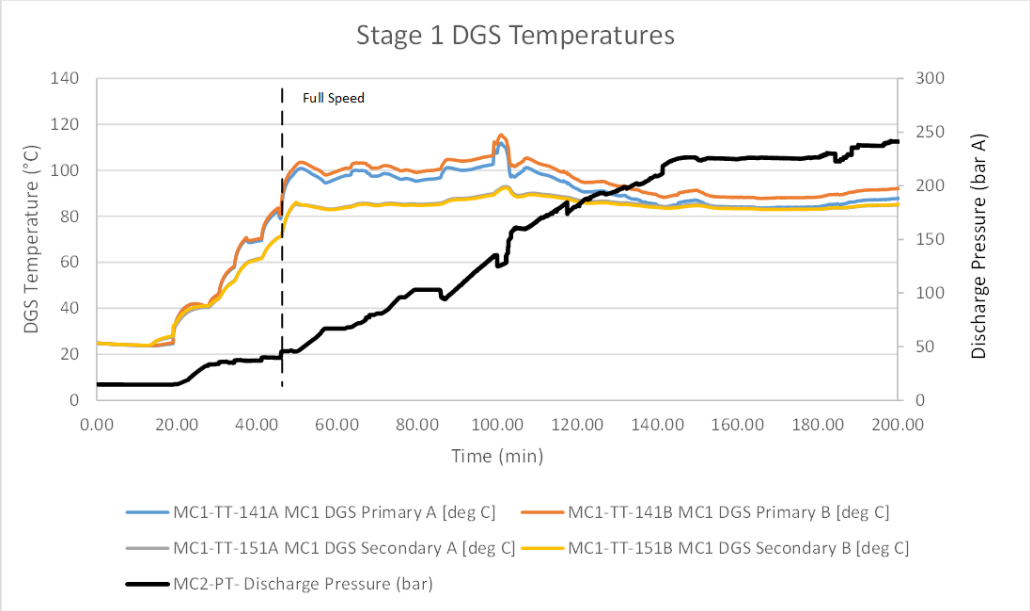

Figure 28. Plot of Compressor Stage 1 DGS Temperatures During Three-Hour Test

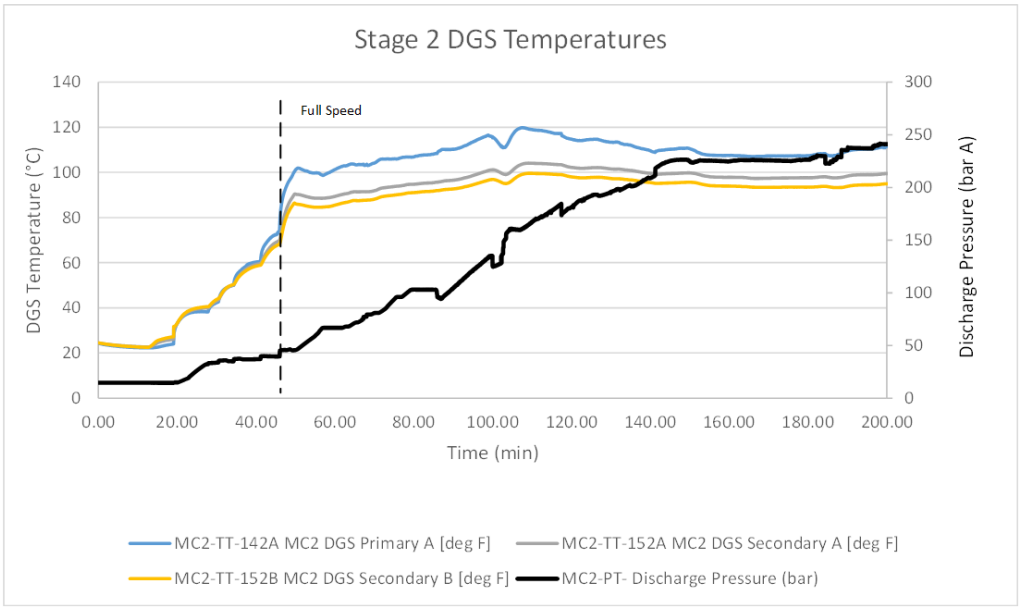

Figure 29. Plot of Compressor Stage 2 DGS Temperatures During Three-Hour Test

COMPRESSOR PERFORMANCE

sCO_2 compressors operate in a region where small changes in temperature result in large changes in enthalpy, see Figure 30 red zone. Typical compressors operate in regions where large changes in temperature result in small changes

in enthalpy, Figure 30 blue zone. Additionally, as compressors are tested near the dome, there is a greater possibility that local accelerations of flow at the inlet of the machine lead to separation of the flow that results in a pressure drop where two phase flow, changes in mach number, and possible choke occur. The sCO_2 compressor discussed here was tested in both locations, as testing in the different zones led to a greater understanding of the machine as compared to testing solely at the design point located in the red zone.

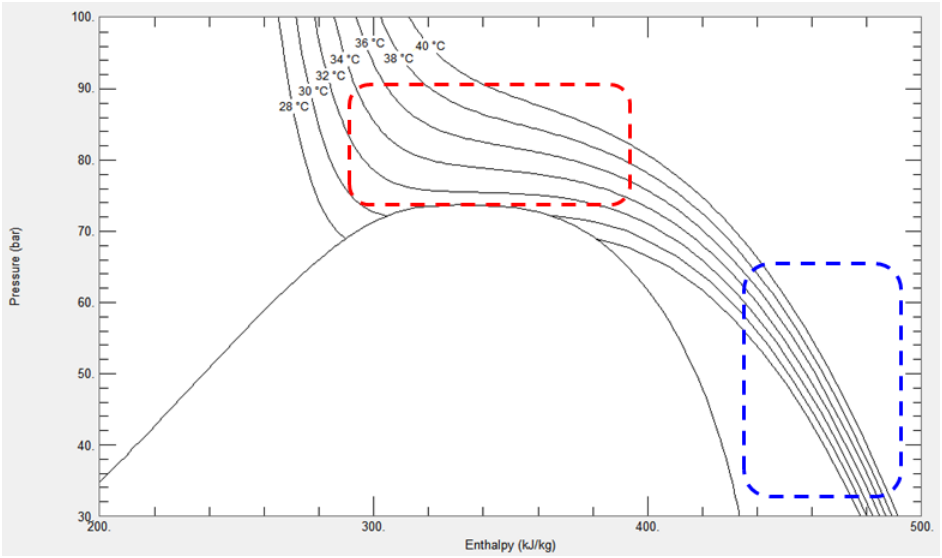

Figure 30. P-H diagram for CO_2 showing how the enthalpy becomes very sensitive to temperature near the critical point.

Figure 31 depicts the Stage 1 head-versus-flow coefficient curve recorded during performance testing relative to the predicted head vs. flow coefficient. An operating range of 69.5% was demonstrated during testing at 30 bar, relative to the design target of >70%, Figure 31, where range is defined as:

$$Range = \frac{\dot{m}_{choke} - \dot{m}_{surge}}{\dot{m}_{choke}}$$

It should be noted that while the machine was designed for operation on the red zone in Figure 30, the CO2 acts much closer to an ideal gas when operating in the blue zone. This allowed our team to assess two characteristics of the compressor. One, our team was able to assess the range of the machine in a region where changes in gas properties were relatively constant. This provides a benchmark that can be assessed using standard 1D methods where we have good reference to experience and to the literature. Two, this provides us with an opportunity to measure the performance with higher accuracy, as results shown later will indicate that at the design point of 37°C, the uncertainty measurement for the impeller performance is quite large. Additionally, determining the range at lower pressure reduces the risk that finding the surge line will lead to damage of the machine, as the pressure and thrust reversals accompanying surge increase with density and operating pressure. It should be noted that the actual range is probably greater than shown in Figure 31 since the authors did not intentionally surge the machine during testing in an effort to prevent damage.

After verifying the stable operating range of the compressor, it was successfully tested at the design inlet conditions of 85 BarA and 37°C. Operation of the unit was initiated at low pressure and mass was added to the loop until design test pressure was achieved. Figure 32 shows the head coefficient and efficiency of the Stage 1 compressor operating near the design flow rate at a range of different inlet pressures. Typically, the efficiency of a centrifugal compressor remains nearly constant at a fixed flow coefficient, even with changes in inlet temperature and pressure. The efficiency of the first stage main compressor is shown in Figure 32, as calculated from the measured temperatures and pressures. Calculating the efficiency following this method based on measured temperature suggests a dramatic decrease in performance with increasing inlet pressure and density. Since the corresponding head coefficient was almost unchanged over the same range of inlet conditions, we can conclude that the efficiency trend is not correct and the

observed trend is a reflection of high uncertainty in the calculated gas enthalpy that accompanies the temperature measurement.

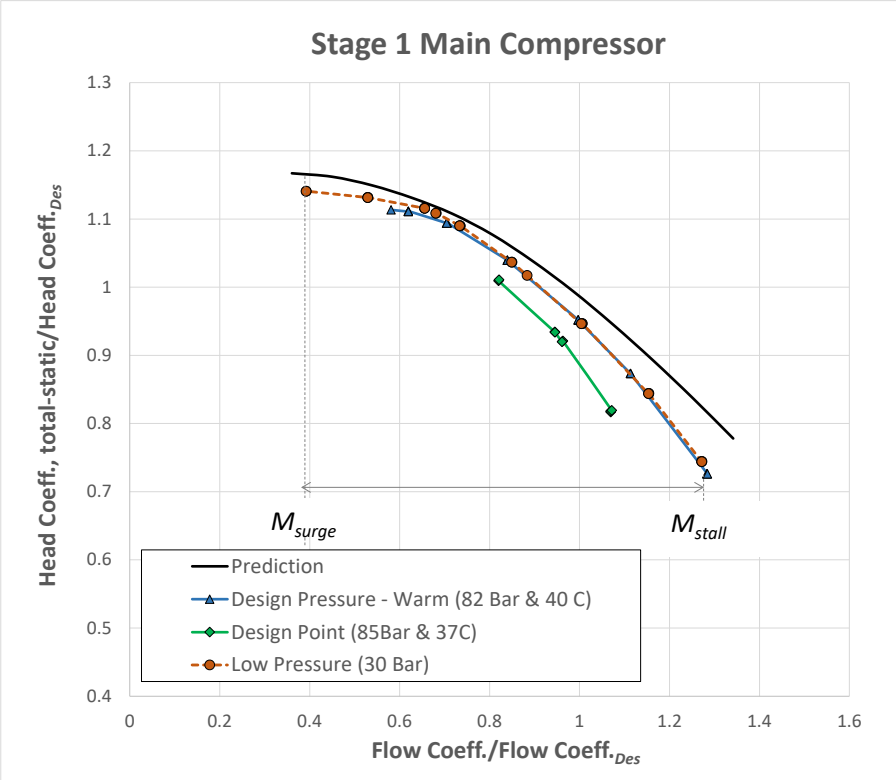

Figure 31. Stage 1 Main Compressor Operating Range

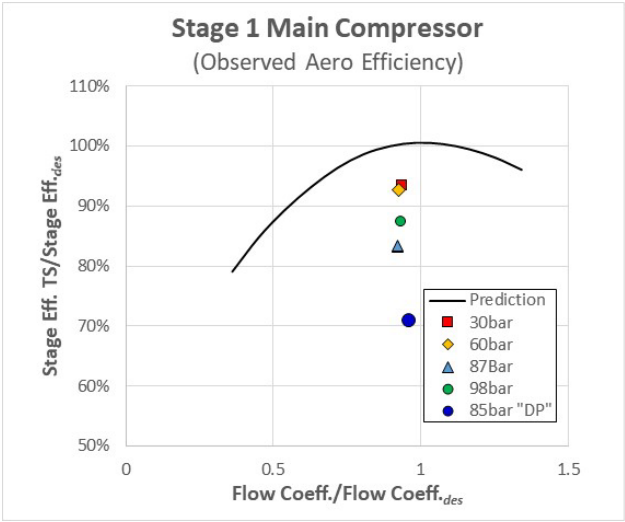

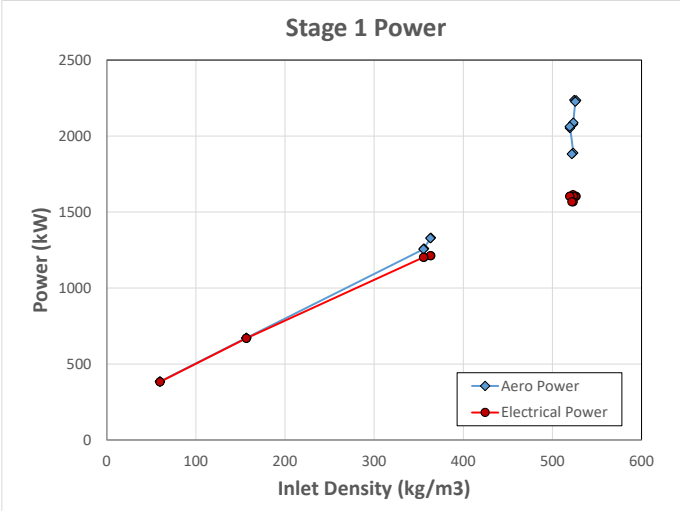

Figure 32. Stage 1 main compressor efficiency and head coefficient.

This sensitivity of compressor efficiency to temperature was anticipated, so provisions were made to calculate efficiency using a power balance. In this approach, the motor power was measured as well as the mechanical losses of the system by instrumenting the lube oil system. This allows the actual work of the compressor to be known. Comparing the measured actual work from the motor power to the isentropic work calculated from the pressure rise, a much more accurate efficiency calculation can be made. This will be explained in further detail in the following paragraphs.

First, to illustrate the challenges with performing performance calculations using temperature and pressure at the inlet and discharge of the compressor using ASME PTC10, an assessment of uncertainty was calculated utilizing a Monte Carlo analysis. For this task, the test team reviewed the data and the procedures used to perform end-to-end calibrations on the test setup, and the team found that based on the end-to-end calibration, the likely 95% confidence for the temperature probes at the inlet and exit of the compressor were approximately 0.1°C. Additionally, the error in the pressure transducers was estimated to be .3 bar based off datasheets. From this data, 10,000 data points were developed for different possible combinations of pressure and temperature at each of the probe locations assuming a normal distribution of error about a nominal design condition. This results in 10,000 combinations for each of the eight temperatures and pressures used to calculate stage one performance. These data are then added to the temperatures measured during a point in the test, and the result then follows a normal distribution in head and efficiency. For efficiency, the 95% confidence interval of the generated data was determined, and the results are shown in Figure 33. As observed, the efficiency measurement even with a temperature uncertainty of 0.1°C is almost 12% uncertainty near 37°C, which is the design point for this machine.

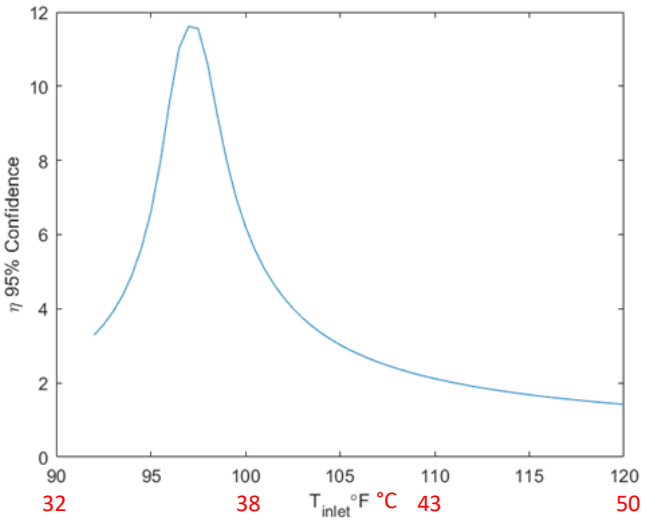

Figure 33. 95% Confidence Interval on Uncertainty as a Function of Compressor Inlet Temperature

There is a reasonably simple explanation for the high uncertainty in efficiency measurement that peaks at 36°C, as illustrated in Figure 34. At approximately 80 bar inlet pressure, C_p increases dramatically at 36°C from 2-3 kJ/kg-K to 30 kJ/kg-K. Thus, very small changes in measured inlet temperature yield very large changes in inlet enthalpy. In other words, measuring the state point at the inlet of the compressor using temperature is not accurate. This observation is why further test campaigns for this compressor utilized a density meter in conjunction with a pressure sensor to measure the state point at the inlet of the compressor. This improves the uncertainty substantially as noted in [13].

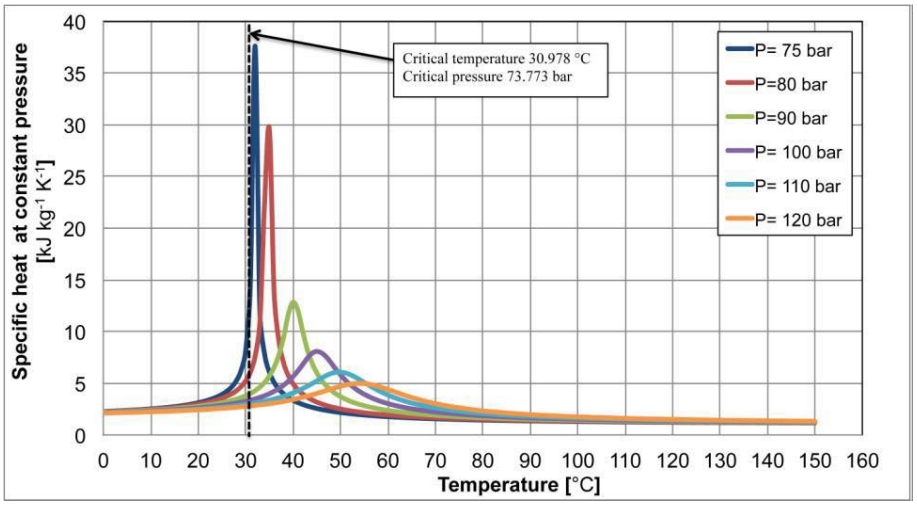

Figure 34. Specific heat at constant pressure versus temperature

Based on the motor power measurements, the compressor efficiency was found to be fairly constant across the range of tested inlet conditions; however, there was some reduction in efficiency near the critical point. The following section shows efficiency measurements as obtained by utilizing a power balance in the compressor. Additionally, the authors added compressor suction density measurements and reported data in a related publication [13].

Eye Seal Improvement

The Build 2 testing revealed that Stage 1 main compressor performance was slightly lower than target. A review of the performance data concluded that there were two primary causes to the shortfall in efficiency. First, higher than

expected eye seal leakage, and second, higher that design impeller passage surface roughness.

A detailed CFD analysis of the Stage 1 compressor front cavity and eye seal was completed to evaluate the as-built configuration. The baseline eye seal design of Stage 1 was estimated to have a leakage rate of ~6.2% of the overall stage flow as shown in Figure 35. Several iterations of seal designs were evaluated and an alternate was selected, which was expected to reduce the leakage rate to 2.8% of total throughput. A similar review and modification to the Stage 2 compressor eye seal was also made to help improve the performance of that stage as well.

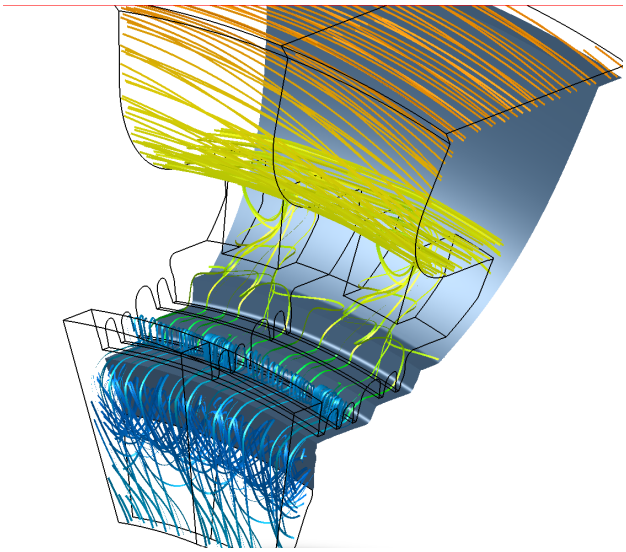

Figure 35. CFD Analysis of the Baseline Eye Seal and Shroud Cavity for Stage 1

Test Build 3: Mar-April 2021

The core was rebuilt for testing of the expander following the results presented above (from Dec 2020) compressor testing with the modified Stage 1 and 2 impellers. In this build the revised compressor eye seals were implemented, as well as an improved surface finish in the flow passages through additional extrude hone finishing. After the compressors were modified and the unit was rebuilt, Build 3 was operated to full pressure and temperature at the expander inlet. The compressors were operated at supercritical conditions close to the design point as required to deliver the intended pressure to the expander. Figure 36 shows that the performance of the Build 3 compressor was significantly improved relative to Build 2 with rougher blades and inferior eye seals. The head coefficient of Stage 1 was increased by 4-5% and the efficiency improved by 4-5 points.

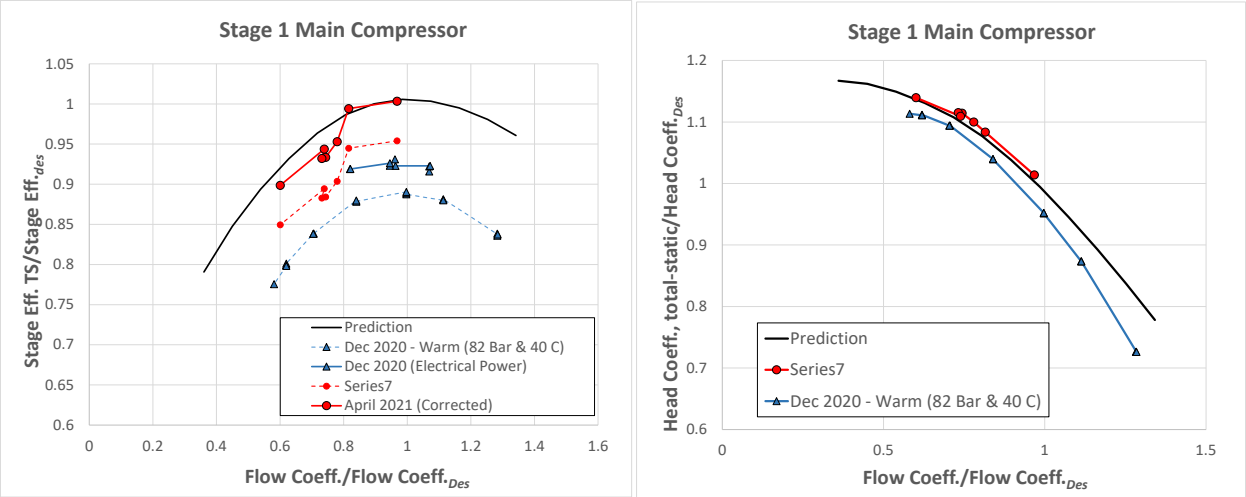

Figure 36. Build 3 Stage 1 Main Compressor Performance.

Stage 2 performance improved even more dramatically compared to the improvement in Stage 1. The improved eye seal and smoother flowpath resulted in a 10 point improvement in efficiency and a 15% increase in head coefficient as shown in Figure 37. Since stage 2 is a very low flow coefficient stage the leakage and frictional losses are more significant, and even small improvements to the configuration yielded significant performance gains.

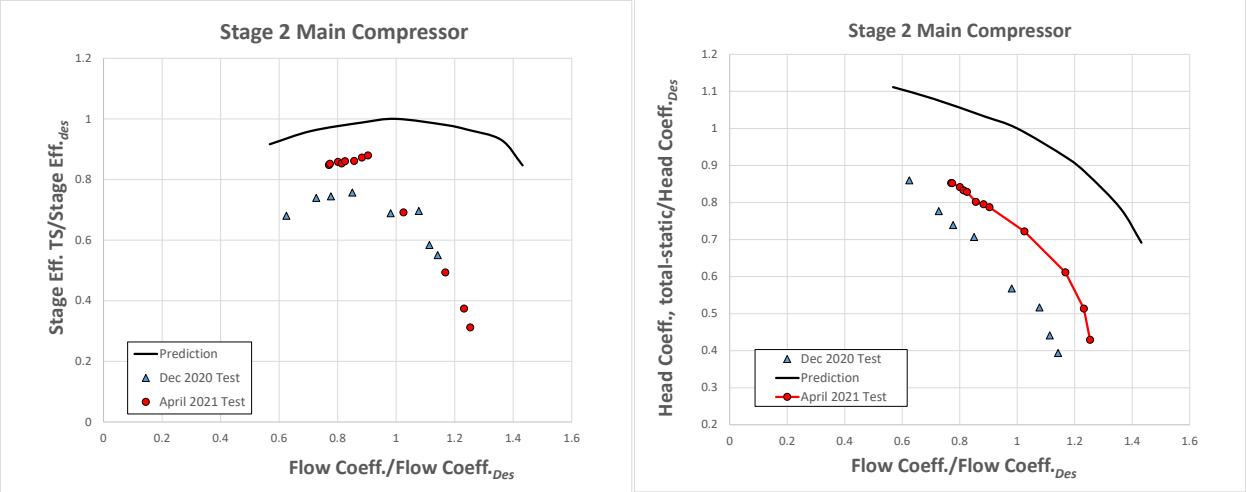

Figure 37. Build 3 Stage 2 Main Compressor Performance

CONCLUSIONS

Overall, this paper presents a summary of the operating constraints, capabilities, and performance for an integrally geared sCO_2 recompression cycle. The results shown in this work suggest that sCO_2 energy conversion devices are predicted to offer very high efficiencies, and are amenable to a variety of heat sources. Numerous projects have been funded to investigate both the techno-economic viability of sCO_2 units, as well as the design variations of these units. Tests described here show successful compressor tests with measured efficiencies approaching targets that yield thermal-to-electric cycle efficiencies of nearly 50% if a turbine inlet temperature of 700°C is achieved. Additionally, this program demonstrated the operation of the compressor across a range of conditions. The vibration, mechanical health, and post test inspection supports further development. The work presented in this paper are inclusive of compressor only test results that were obtained during a DOE supported grant. Since completion of this DOE program, this unit has been operated in a compressor test configuration and in a turbine test configuration for over 100 hours of additional testing.

REFERENCES

[1] Wilkes, J., Allison, T., Schmitt, J., Bennett, J., Wygant, K., Pelton, R., Bosen, W., 2016, Application of an Integrally Geared Compander to an sCO_2 Recompression Brayton Cycle, The 5th International Symposium - Supercritical CO_2 Power Cycles, March 29-31, San Antonio, Texas.

[2] System Advisor Model Version 2016.3.14 (SAM 2016.3.14). National Renewable Energy Laboratory. Golden, CO. Accessed October 31, 2016. https://sam.nrel.gov/content/downloads.

[3] Schmitt, J., Wilkes, J., Allison, T., Bennett, J., Wygant, K. and Pelton, R., "Lowering the Levelized Cost of Electricity of a Concentrating Solar Power Tower with a Supercritical Carbon Dioxide Power Cycle," GT2017-64958, Proceedings of ASME Turbo Expo 2017, June 26-30, 2017, Charlotte, NC.

[4] Numerical Propulsion System Simulation (NPSS), http://www.swri.org/npss/.

[5] Lemmon, E.W., Huber, M.L., McLinden, M.O. NIST Standard Reference Database 23: Reference Fluid Thermodynamic and Transport Properties-REFPROP, Version 9.1, National Institute of Standards and Technology, Standard Reference Data Program, Gaithersburg, 2013.

[6] Neises, T. and C. Turchi, "Supercritical CO_2 Power Cycles: Design Considerations for Concentrating Solar Power," The 4th International Symposium – Supercritical CO_2 Power Cycles, September 9-10, 2014, Pittsburgh, PA.

[7] "SunShot Vision Study", U.S. Department of Energy, February, 2012, DOE/GO-102012-3037, Prepared by National Renewable Energy Laboratory, Accessed 2015, http://www1.eere.energy.gov/solar/pdfs/47927.pdf.

[8] Hoopes, K., Sanchez, D., Crespi, F., 2016, A New Method For Modelling Off-Design Performance of sCO_2 Heat Exchangers Without Specifying Detailed Geometry, The 5th International Symposium - Supercritical CO_2 Power Cycles, March 29-31, San Antonio, Texas.

[9] Deb, K., Pratap, A., Agarwal, S., "A Fast and Elitist Multiobjective Algorithm: NSGA-II", IEEE Transactions on Evolutionary Computation, Vol. 6, No. 2, Aril 2002.

[10] Ashvin Hosangadi, Tim Weathers, Zisen Liu, Robert Pelton, Karl Wygant, and Jason Wilkes, 2021, "Numerical Predictions of Mean Performance and Dynamic Behavior of a 10 MWe sCO2 Compressor with Test Data Validation," GT2022-82017, *Proc. of ASME Turbo Expo 2022*, June 13-17, 2022, Rotterdam, the Netherlands.

[11] Li, F., Pelton, R., Jung, S., "Mechanical Design of a 3D printed, Semi-shrouded, Centrifugal Compressor for sCO2 Application" GPPS Zurich Forum, GPPS-2018-0064, 2018.

[12] Allison, T., Smith, N., Pelton, R., Jung, S., Wilkes, J., "Experimental Validation of a Wide-Range Centrifugal Compressor Stage for Supercritical CO2 Power Cycles", ASME Journal of Engineering for Gas Turbines and Power, GTP-18-1621, 2018.

[13] Pelton, R., Bygrave, J., Wygant, K., Wilkes, J., Revak, T., Kim, K., 2022, "Near Critical Point Testing and Performance Results of an sCO2 Compressor for a 10 MWe Brayton Cycle," *Proc. Of ASME Turbo Expo 2022*, June 13-17, GT2022-83503, Rotterdam, The Netherlands.

ACKNOWLEDGEMENTS

The authors gratefully acknowledge Hanwha Power Systems for supporting this research, as well as the US Department of Energy, Office of Energy Efficiency and Renewable Energy Project EE0007114.